UNIVERSITY OF CALGARY

Numerical and physical modeling of P-S converted waves in VTI media

by

Jianli Yang

A THESIS

SUBMITTED TO THE FACULTY OF GRADUATE STUDIES

IN PARTIAL FULFILLMENT OF THE REQUIREMENTS FOR THE

DEGREE OF MASTER OF SCIENCE

DEPARTMENT OF GEOLOGY AND GEOPHYSICS

CALGARY, ALBERTA
September, 2003

THE UNIVERSITY OF CALGARY
FACULTY OF GRADUATE STUDIES

The undersigned certify that they have read, and recommended to the Faculty of Graduate Studies for acceptance the thesis entitled "**Numerical and physical modeling of P-S converted waves in VTI media** " submitted by Jianli Yang in partial fulfillment of the requirements for the degree of Master of Science.

Supervisor, Dr. Don C. Lawton
Department of Geology and Geophysics

Co-supervisor, Dr. Edward S. Krebes
Department of Geology and Geophysics

Dr. Laurence R. Lines
Department of Geology and geophysics

Dr. S.A. (Raj) Mehta
Department of Chemical and Petroleum Engineering

Date

ABSTRACT

The earth's crust is not isotropic as is traditionally assumed, but is anisotropic and inhomogeneous. Vertical Transverse Isotropy, also called polar anisotropy with vertical axis, is the most commonly considered type of velocity anisotropy. Converted wave (P-S) analysis in VTI media was conducted, focusing on conversion point mapping. It was found that the location of P-S conversion point in VTI media depends on the anisotropic parameters ε and δ, V_P/V_S and offset/depth. When ε is larger than δ, for the same offset, the conversion point moves towards the source in VTI media relative to that in the isotropic case. The displacement of the conversion point from that in the isotropic case increases with the increasing offset-to-depth ratio and the value of ε. The velocity ratio doesn't have a significant influence on the displacement of the conversion point for small offset/depth, but has an influence on for large offset/depth. The P-S conversion point was also calculated by using the γ_{eff} method and compared with the results obtained from raytracing method. It is found that for long offsets, i.e. offset-to-depth ratio greater than 2, the γ_{eff} method is an insufficient approximation for mapping the P-S conversion-point.

A 2C (P-P and P-S) seismic survey was designed and conducted on a scaled VTI physical model and data were acquired and processed. It is shown that the overburden VTI layer does not have significant influence on P-P imaging. When isotropy is assumed in P-S data processing, the slab edge position obtained has a lateral shift from its true position.

ACKNOWLEDGEMENTS

I would like to thank my supervisor Dr. Don C. Lawton for his great encouragements and guidance during my study. He guided me by his insightful ideas and serious academic attitude to do research. I would also like to thank my co-supervisor, Dr. Edward Krebes for his help on understanding geophysical theories and authorization to use his code.

I thank Eric Gallant and Henry Bland for establishing the physical model and conducting the measurements. I am also thankful to Hanxing Lu and Kevin Hall for their help on solving technical problems when I was using ProMAX. I am also grateful to Dr. Larry Lines and Dr. Jim R. Brown for their valuable suggestions, and David Henley for his assistance in using his radial trace filters. I also want to express my deep appreciation to all CREWESERS for their kind help.

The financial support of CREWES is greatly appreciated.

Thanks to my parents and my parents-in-law for their great support.

To my husband Du Jian

TABLE OF CONTENTS

LIST OF FIGURES

LIST OF TABLES

LIST OF SYMBOLS AND ACRONYMS

CCP	Common Conversion point
VTI	Vertical Transverse Isotropy
NMO	Normal MoveOut
σ_{ij}	stress tensor
u	particle displacement
C_{ijkl}	stiffness tensor
e_{ij}	strain tensor
μ	shear modulus or rigidity
λ	incompressibility
V_P	compressional wave velocity
ε	P-wave anisotropy parameter defined by Thomsen
δ	P-wave anisotropy parameter defined by Thomsen
γ	SH wave anisotropy parameter defined by Thomsen
A_I	amplitude of incident P-wave
A_T	ampliude of transmitted P-wave
A_R	amplitude of reflected P wave
B_R	amplitude of reflected S-wave
B_T	amplitude of transmitted S-wave
θ_1	P-wave incident angle
θ_2	P- wave transmitted angle
ϕ_1	S-wave reflective angle
ϕ_2	S-wave transmitted angle
ρ	density
ΔV_P	difference of P velocities on both sides of an interface
ΔV_S	difference of S velocities on both sides of an interface
α_0	P-wave velocity in vertical direction
β_0	S-wave velocity in vertical direction
θ	phase angle

ϕ	ray angle
p	ray parameter
V_P	P wave velocity
V_S	S wave velocity
θ_P	P-wave incident angle
ϑ_S	S-wave reflective angle
R_{PSV}	reflection coefficient at any incident angle for P-wave incidence and SV wave reflection.
x_C	conversion point offset from the source
x_{C0}	asymptotic conversion point offset
x	source-receiver offset
t_P	one-way oblique traveltime for P-wave
t_S	one-way oblique traveltime for S-wave
γ_{eff}	effective velocity ratio
γ_0	vertical velocity ratio
γ_2	ratio of short-spread P-wave moveout velocity to the S-wave corresponding

Chapter one:

Introduction to anisotropy and converted waves

1.1 Introduction

In traditional seismic exploration, the earth's crust is assumed to be isotropic. Isotropy means that a particular physical property is identical in every direction. However, the subsurface layers are not generally the ideal and simple case that we assume. Seismic velocity anisotropy is widely seen in our exploration activities and has been measured in shales and fractured rock formations. Researchers have found that the anisotropy of geological formations cannot be neglected in some areas. "Getting a grip of anisotropy of the earth can mean the difference between success and failure in reservoir evaluations and development" (Anderson et al., 1994).

Conventional seismic data processing is based on the assumption that the media in which waves propagate is isotropic. With acceleration of computational speed, research on anisotropy has become more feasible. However, due to the complexity of general anisotropy, it has previously not been included in general seismic exploration. Recently, most of the work done on the anisotropy has been concentrated on a particular type of anisotropy, known as Vertical Transversely Isotropic (VTI).

Several authors have shown the effect of anisotropy on seismic exploration. Larner and Cohen (1993) and Alkhalifah and Larner (1994) investigated the migration error in transversely isotropic model with different dipping reflectors. They found the mis-positioning error behaviour depends on the anisotropy parameters. They concluded the key to success in migration in the presence of anisotropy is the use of an algorithm that not only honours anisotropy, but also uses good estimates of the anisotropy parameters. Vestrum et al. (1998) developed anisotropic depth-migration approach for P-wave seismic data in TTI media, which is a transversely isotropic medium with tilted symmetry axis. They also applied anisotropic migration to the physical-model seismic data and field seismic data from Canadian Rocky Mountain Thrust and Fold Belt. They found that if anisotropy is ignored, the seismic anisotropy in dipping shales causes imaging and mis-positioning problems on the structure below it. Isaac and Lawton (1999) conducted physical modeling in (TTI) model, and showed that a TTI overburden caused a dramatic lateral-shift on imaging of targets underneath.

Multi-component seismic recording, specifically P-S converted waves, has been developing rapidly in recent years for exploration for subsurface targets. Because it captures the seismic wavefield more completely than conventional single-element techniques (Stewart et al., 2002), it is beneficial for structural imaging, lithology estimation and anisotropy analysis, subsurface fluid description, and reservoir monitoring (Stewart et. al. 2003). However, most of previous work on multi-component seismology has not taken anisotropy into account. Anisotropy effects on P-wave seismic data are often small and difficult to attribute convincingly to anisotropy. However, anisotropy effects are significant on P-S converted wave data interpretation (Winterstein, 1990).

The main purpose of this thesis is to discover the effect of anisotropy (particularly the VTI case) on P-S converted wave mapping and imaging. In this chapter, the basic concepts of seismic anisotropy and the VTI case will be reviewed. Then the principles and application of converted-wave exploration will be summarized briefly. Then the specific objectives of the research and a summary outline of the thesis will be presented.

1.2 Review of seismic anisotropy

The subject of anisotropy has a long history but now has come to be a central feature of geophysics to explore hydrocarbons (Thomsen 2002). "It can be said that any process which involves the concept of scalar velocity field is subject to error if, in fact, the actual velocity is a vector whose magnitude depends upon its direction."(Tsvankin, 1999). By definition, anisotropy means the variation of a physical property depending on the direction in which it is measured. In the field of our interest, seismic anisotropy is defined to be the dependence of seismic velocity on either the direction of travel or the direction of polarization (Sheriff, 2002). Seismic velocity here includes not only the P-waves, but also the other waves (e.g. S-waves).

Accounting for the effects of anisotropy of the earth begins with understanding the geologic foundations of anisotropy. Anisotropy in sedimentary rocks may be caused by various factors (Thomsen 1986 and 2002):

(a) Thin isotropic or anisotropic layers
(b) Preferred orientation of anisotropic mineral grains
(c) Preferred orientation of cracks and flat pores (sandstones)

These attributes can exist in the rocks independently or in combination. The isotropic materials can display anisotropy due to fine layering. Carbonates can display anisotropy due to the oriented distribution of cracks. Anisotropy seldom appears in igneous rocks and metamorphic rocks.

1.2.1 Anisotropy versus heterogeneity

Anisotropy is easily to be confused with heterogeneity by many people since both terms are used to characterize velocity variation within rock formations. The distinction between these two terms has to be made clear. Heterogeneity is defined as the variation of a certain physical property from point to point. However, the anisotropy means the directional variation of a certain physical property at one point. The figure 1.1 shows the distinction between heterogeneity from anisotropy.

However, heterogeneity may be related to anisotropy by using different scales. For example, a rock sample, sandstone or shale, is heterogeneous at the grain scale. The grains can have an order, a fabric or a texture, which makes the rock block appears to be anisotropic. This order may be caused by sedimentation. It is this ordered heterogeneity on the small scale, which causes seismic anisotropy on the large scale. Anisotropy and heterogeneity may coexist. There are four possible conditions: isotropic and homogeneous, isotropic and heterogeneous, anisotropic and homogeneous, and anisotropic heterogeneous. The real earth is known as being both heterogeneous and anisotropic.

Homogeneous and isotropic **Heterogeneous and isotropic**

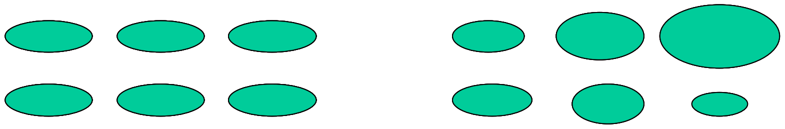

Homogeneous and anisotropic **Heterogeneous and anisotropy**

Figure 1.1 Distinction between anisotropy and heterogeneity (After R. J. Brown, 2001).

The standard of large or small scale means whether the seismic wavelength is larger or smaller than the heterogeneity scale. When the seismic wavelength is large compared to the size of the heterogeneous object, the object can be considered as a homogeneous, anisotropic one (Backus, 1962). In this case, the waves obey the laws of anisotropic wave propagation (Thomsen, 2002).

1.2.2 VTI (Polar Anisotropy)

In seismic exploration, the most commonly considered type of anisotropy is polar anisotropy, which is also called Transverse Isotropy (TI). It has a symmetry axis and typically the axis is perpendicular to bedding. The velocities on the plane normal to this axis are identical. When this symmetric axis is vertical, the medium is called Vertical Transversely Isotropic (VTI) and isotropy is limited within the horizontal plane. For example, a set of horizontal thin-bed shale belongs to VTI case. The velocity distribution in VTI can be shown schematically by a cylinder (Figure 1.2). This type of anisotropy is important in sedimentary basins, and is also the media that this thesis going to discuss.

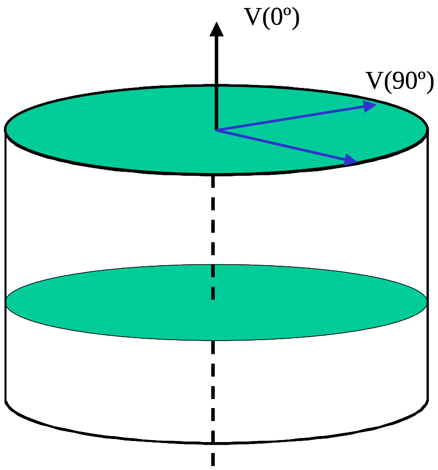

Figure 1.2 Velocity distribution in VTI media can be represented by a cylinder. The velocities on all directions within the horizontal plane are identical in amplitude.

When the symmetry axis is not vertical, the case is termed as Tilted Transversely Isotropic (TTI). When the symmetry axis is horizontal, it is called Horizontal Transversely Isotropic (HTI), or horizontal polar anisotropy. In this case, the isotropy is constrained within the vertical plane. HTI media corresponds to the vertical tilted beds or to the case of vertical fractures in isotropic formation.

1.3 Review of P-S converted wave seismic exploration

The primary traditional seismic exploration method is the P- wave reflection survey. The compressional P- wave arrives at the receiver first among all elastic waves, and usually has a high signal-to-noise ratio (Stewart et al., 2002). It is easy to be generated by a variety of sources, and can propagate in fluid environments. However, P- wave images cannot provide enough information and more wave information is needed to obtain a better image. Multi-component seismic surveys, normally 3 components, were developed to assist P-wave exploration for it can provide additional information about the subsurface. These surveys capture not only the compressional P-P reflections, but also P-S converted waves. This method was proposed and tried in late 1970s, and has been proceeding for about 20 years. Now several commercial acquisition and processing groups are now active in this field and the technology is becoming mature.

1.3.1 Method

When we use the term “converted-wave exploration”, we imply a particular conversion: a downward-propagating P-wave, converting on reflection at its deepest point of penetration to an upward-propagating S- wave (Stewart et. al., 2002).

The raypath of a P-S converted wave is shown in Figure 1.3, with the bold arrows showing the positive phase direction. The P-S ray path is asymmetric due to Snell’s law:

$$\frac{\sin\theta_P}{V_P} = \frac{\sin\theta_S}{V_S} \tag{1.1}$$

where θ_P and θ_S are the P-and S-wave angle of incidence and reflection, respectively, and V_P and V_S are the P- and S-wave velocities, respectively.

Since $V_P > V_S$, θ_P is greater than θ_S, so the S-wave is closer to a vertical direction than the incident P-wave. The geometry of P-S converted wave is determined by Snell's law, and the amplitude is given by Zoeppritz equations, which will be discussed in Chapter 2.

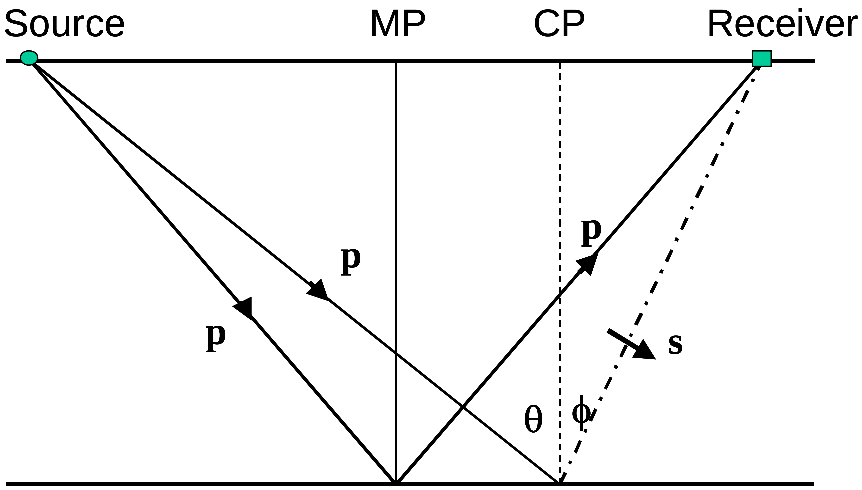

Figure 1.3 A converted wave (P-S) reflection at its conversion point (CP) compared with a pure P-wave reflection at its mid-point (MP). Note that the CP is shifted towards the receiver. (After Stewart et. al., 2002).

Stewart et al. (2002) summarized the principles of P-S exploration by comparison with the conventional P-P method. Survey design for acquiring P-S data is similar to P-P data, but must take V_P/V_S into consideration for the asymmetric ray path. P-S surveys use conventional sources, but require more recording channels per receiver location.

Some special processing work has to be done to obtain the correct P-S image, which include anisotropic rotations, S-wave receiver statics, asymmetric and anisotropic binning, non-hyperbolic velocity analysis and NMO correction, P-S to P-P time transformation, P-S dip moveout, prestack migration with two velocities and wavefields, and stacking velocity and reflectivity inversion for S-wave velocities. Interpretation of P-S- sections uses full elastic raytracing, synthetic seismograms, and correlation with P-wave sections.

1.3.2 Applications

During the past 20 years, since P-S exploration was introduced, it has been applied broadly in providing additional formation information to the P-wave section. It has been proved that this method is effective in several aspects (Stewart et al., 2003). P-S wave analysis has been applied to structural imaging, e.g. seeing through the gas-charged sediments and improving near-surface resolution.

Figure 1.4 shows an example of P-P and P-S images of gas-saturated structure in the North Sea. Reflections from the interface within and below the gas-charged channels are poor on P-wave section (Figure 1.4 a). In contrast, the P-S section (Figure 1.4 b) delineates the channel bases, interface below the channel and sediment boundaries within the channel. P-waves are sensitive to gas-saturation and S-waves are sensitive to rock matrix properties. So, S-waves can penetrate gas-saturated sediments, while the P-P reflections from the interfaces within and below the gas-charged channels are poor.

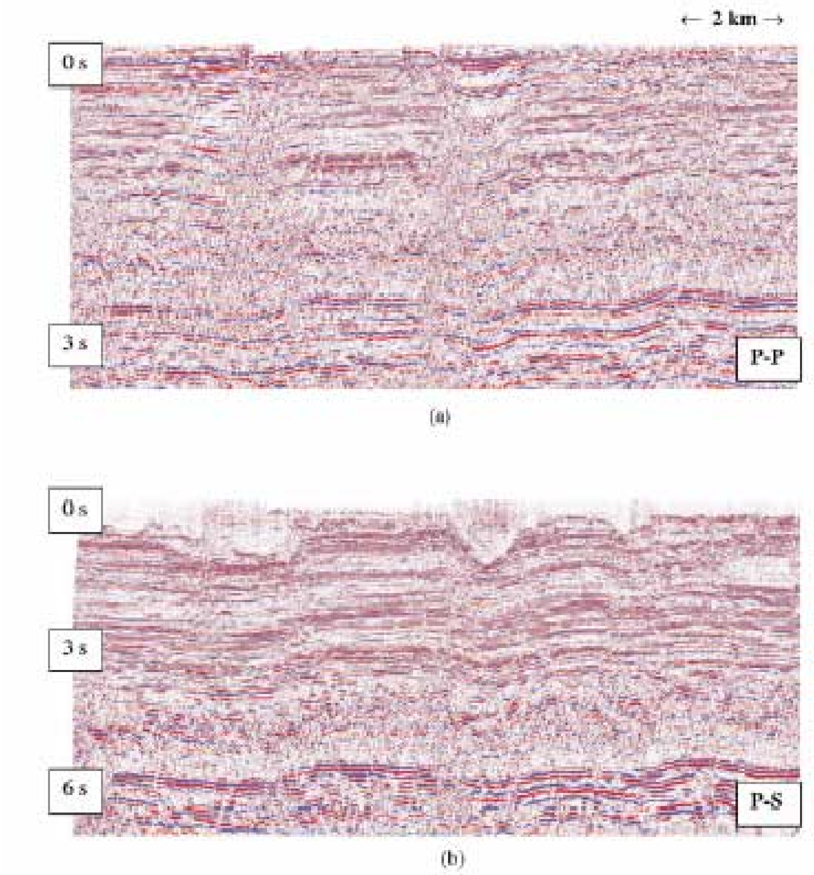

Figure 1.4 Comparison between (a) P-wave and (b) P-S 2D seismic over North Sea shallow-gas channels. (Courtesy WesternGeoco, from Stewart et al. 2003)

P-S wave sections can also provide additional information about lithology estimation (Helbig 1986). Much of P-S analysis is targeted at finding an S-wave velocity or determining a V_P/V_S value (e.g., Li et al., 1999). Both V_S and V_P/V_S are good indicator of rock type, especially when combined with V_P (Tatham, 1982). Figure 1.5 displays a chart for lithology identification with V_P and V_P/V_S (Miller and Stewart, 1990). Garotta et al. (1985) analyzed the P-P and P-S data for a Viking sand channel reservoir in Winfield oil field, Alberta. They used P-P and P-S isochron ratios around the area of interest to determine V_P/V_S and Poisson’s ratios, which is a good indicator for distinguishing sand from the neighbouring shales.

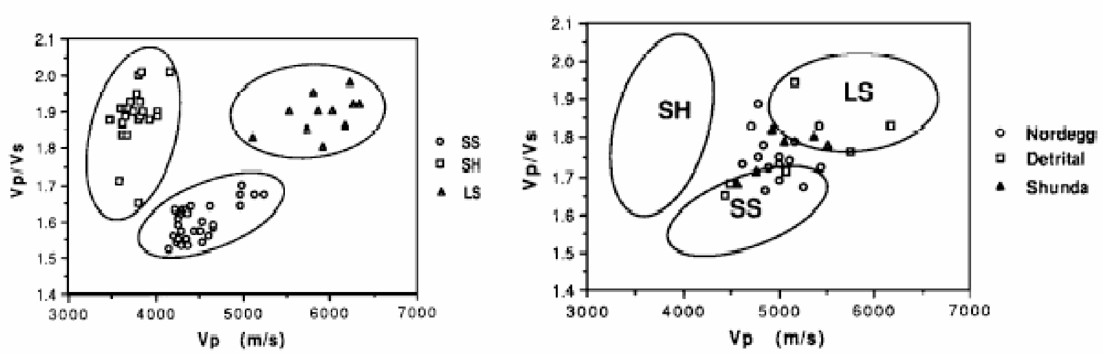

(a) (b)

Figure 1.5 (a) Well-log V_P/V_S versus V_P for pure lithologies of the Medicine River field. (b) V_P/V_S versus V_P for mixed lithologies (From Miller and Stewart, 1990). SS=sandstone, SH=shales, and LS=limestone. Nordegg, Detrial, and Shunda are litholostratigraphafic units.

P-S exploration has also been used for anisotropy analysis (Gaiser, 2000, Li et al., 1996) to predict the fracture density and orientation. The V_P and V_S values obtained from inversion plus well logs can be applied to predict porosity values (Thompson et al., 2000, Stewart and Todorov, 2000) and water saturation using a neural net.

1.3.3 Significance of the conversion point location in 3C exploration

The area of coverage and resultant fold of a 3-D seismic survey are fundamental parameters in survey design (Stewart, 1999). It has been shown (Thomsen, 1999) that anisotropy has a significant influence on the 3C seismic survey design, P-S converted wave processing, and subsurface imaging. In 3D-3C survey design, due to the asymmetry of the P-S ray path, the conversion points are distributed irregularly at the reflector (Cordsen and Lawton, 1996). If nearest binning method is applied, this irregularity could cause high frequency (bin-bin) fold variations in P-S maps (Lawton and Cary, 2000). If the sedimentary section is anisotropic, the anisotropy may affect the location of the depth-variant conversion point.

The P-S conversion point position in anisotropic media, especially in VTI media, has to be calculated carefully. The dependence of the P-S conversion point position on anisotropy parameters, V_P/V_S and other factors, is a primary focus of this thesis.

1.4 Structure of the thesis

The main objective of this thesis is to discover the influence of anisotropy on the location of the P-S conversion points, through forward ray tracing and physical modeling imaging. It includes two parts: numerical modeling and physical modeling.

1.4.1 Part one: Numerical modeling

In Chapter 2, the elastic anisotropic strain-stress equations, and relevant wave equations will be introduced. The anisotropy tensor and matrix will be displayed and TI media will be defined mathematically. Three defined scalar anisotropic parameters will be introduced, and reflection and transmission coefficients in a VTI model will be calculated and compared with the isotropic case.

In Chapter 3, Thomsen's equation to calculate angle-dependent velocities will be introduced. A single-layer VTI model is created, and an algorithm is designed to map the converted wave, focusing on the location of P-S conversion point. The displacement of the conversion point from its location in isotropic case will be calculated and displayed. The dependence of this displacement on anisotropic parameters, the velocity ratios, and the offset/depth ratio will also be discussed.

In Chapter 4, the commercial anisotropy ray mapping software, NORSAR2D, will be tested to map the P-S converted waves in VTI media. These mapping results are compared and displayed. Also another ray-mapping approximation method, the effective velocity ratio method, will be introduced and applied in both a single layer model and a three-layer model. The relative error of this approximation method will be calculated and then discussed.

1.4.2 Part two: physical modeling experiment and imaging

In Chapter 5, a scaled physical model will be constructed and both P-P and P-SV seismic surveys will be recorded on the model. This physical model is composed of a VTI block with an isotropic slab affixed underneath. The edge of the slab is used to simulate a reef edge or a fault. The P-P and P-SV data will be acquired and processed by using ProMAX and taking the anisotropy into consideration. The processed image is then compared and the mis-positioning of the location of the step is then calculated.

In Chapter 6, a general discussion and conclusion from the thesis is summarized.

Chapter two:

Reflection and Transmission of converted waves in VTI media

2.1 Chapter summary

As mentioned in chapter one, seismic anisotropy is defined as the velocity dependence on direction. The media where the wave propagates is not as simple and ideal as in the isotropic case. This means that we have to probe the theory for more general anisotropy, especially for the VTI case.

Since this thesis consists of P-S numerical modeling in VTI media, the main objectives include calculating the amplitude of reflection and transmission coefficients on the interface, and the horizontal conversion point location on the interface. These parameters have to be calculated correctly.

In this chapter, the thesis will focus on computing the reflection and transmission coefficients of VTI media. The theory of anisotropic media, which includes the elastic strain-stress equation, and the wave equation, will be reviewed. The reflection and transmission coefficients will be calculated and compared with the isotropic case.

2.2 Theory

2.2.1 Elastic strain-stress equation and wave equation

In elastic medium, there exists a linear relationship between strain and stress (force per unit area), which is Hooke's Law. In the anisotropic Hooke's law, each component of stress σ_{ij} is assumed to be linearly proportional to all the components of the strain e_{ij} as following equation (Nye, 1957):

$$\sigma_{ij}(x,t) = \sum_{k=1}^{3}\sum_{l=1}^{3} C_{ijkl} e_{kl} = \sum_{k=1}^{3}\sum_{i=1}^{3} C_{ijkl} \frac{\partial u\left(\vec{x},t\right)_k}{\partial x_l} \tag{2.1}$$

where $u(x,t)$ is the displacement of a particle at time t and position x, and C_{ijkl} is the tensor of elastic constants, or the stiffness tensor.

At the same time, each particle obeys Newton's Second Law of motion, given by:

$$\rho \frac{\partial^2 u_i}{\partial t^2} = \sum_{j=1}^{3} \frac{\partial \sigma_{ij}}{\partial x_j} \qquad i, j = 1,\ 2,\ 3\,. \tag{2.2}$$

where the subscripts i, j denotes the components of the vectors $\vec{u}$ and $\vec{x}$, and ρ is density. The two subscripts, i, j, define the orientation of a unit area by its normal vector, and the vector component of the force-per-unit, respectively.

Inserting equation (2.1) into equation (2.2), and assuming the medium is locally homogeneous, we can derive the wave equation (Krebes, 2001):

$$\frac{\partial^2 u_i}{\partial t^2} = \sum_{j=1}^{3}\sum_{k=1}^{3}\sum_{l=1}^{3} \frac{C_{ijkl}}{\rho}\frac{\partial^2 u_k}{\partial x_l \partial x_j} \tag{2.3}$$

where C_{ijkl} is the stiffness tensor.

2.2.2 Stiffness tensor and module matrix

In the wave equation, equation (2.3), C_{ijkl} is a $3 \times 3 \times 3 \times 3$ tensor which can be replaced with a 6×6 matrix $\tilde{C}_{\alpha\beta}$ according to the Voigt scheme (Thomsen, 2002).

$$\begin{array}{lccccccc} each\quad index\quad pair & ij = 11 & 22 & 33 & 23 & 13 & 12 \\ maps\quad \mathrm{int}\, o & \downarrow\ \downarrow & \downarrow & \downarrow & \downarrow & \downarrow & \downarrow \\ a\quad \sin gle\quad index & \alpha = \ 1 & 2 & 3 & 4 & 5 & 6 \end{array}$$

The tensor has been converted to the equivalent matrix 6×6 matrix $\tilde{C}_{\alpha\beta}$, which is symmetric, and even the most general kind of anisotropy has at most 21 different elements. In some special symmetric cases, the number of independent elements can be fewer than 21.

In a geophysical survey, we cannot measure all of these elements. Fortunately, for our investigation on anisotropy, we may not need to measure the values of these elements, but only for some independent ones and the relationships between them.

2.2.3 Modula matrix in isotropic case and polar anisotropy

The simplest type of symmetry of the 6×6 matrix, $\tilde{C}_{\alpha\beta}$, is the isotropic case, where most of the elements are zero. There are three different elements and two are independent due to the relationship $\sigma = \lambda + 2\mu$, where λ and μ are Lame constants.

$$\begin{bmatrix} C_{11} & C_{12} & C_{13} & C_{14} & C_{15} & C_{16} \\ C_{21} & C_{22} & C_{23} & C_{24} & C_{25} & C_{26} \\ C_{31} & C_{32} & C_{33} & C_{34} & C_{35} & C_{36} \\ C_{41} & C_{42} & C_{43} & C_{44} & C_{45} & C_{46} \\ C_{51} & C_{52} & C_{53} & C_{54} & C_{55} & C_{56} \\ C_{61} & C_{62} & C_{63} & C_{64} & C_{65} & C_{66} \end{bmatrix} \rightarrow \begin{bmatrix} \sigma & \lambda & \lambda & & & \\ \lambda & \sigma & \lambda & & & \\ \lambda & \lambda & \sigma & & & \\ & & & \mu & & \\ & & & & \mu & \\ & & & & & \mu \end{bmatrix}$$

For the case with polar symmetry, the matrix has 5 independent parameters as following:

$$\begin{bmatrix} C_{11} & C_{11}-2C_{66} & C_{13} & & & \\ C_{11}-2C_{66} & C_{11} & C_{13} & & & \\ C_{13} & C_{13} & C_{33} & & & \\ & & & C_{44} & & \\ & & & & C_{44} & \\ & & & & & C_{66} \end{bmatrix} \rightarrow \begin{bmatrix} \lambda+2\mu & \lambda & \lambda' & 0 & 0 & 0 \\ \lambda & \lambda+2\mu & \lambda' & 0 & 0 & 0 \\ \lambda' & \lambda' & \lambda''+2\mu & 0 & 0 & 0 \\ 0 & 0 & 0 & \mu' & 0 & 0 \\ 0 & 0 & 0 & 0 & \mu' & 0 \\ 0 & 0 & 0 & 0 & 0 & \mu \end{bmatrix}$$

In this case, the two axis 1 and 2 are equivalent each other, but they are different from axis 3. Then the seismic velocity will be independent of direction in the (1,2) plane.

When the 3-axis is vertical, it is called vertical polar anisotropy, or VTI, as introduced in Chapter one. The velocities are of same value in all horizontal azimuths.

2.2.4 Solution of plane waves

The equation of motion, equation (2.3), has to be solved for the case of VTI case. Suppose that the displacement is a harmonic plane wave which has a form of:

$$u_k = U_k \exp\left[i\varpi(\vec{s}\cdot\vec{x} - t) \right] \tag{2.4}$$

where ϖ is the radial frequency, and $\vec{s}$ is the slowness.

The derivatives can be worked out as:

$$\frac{\partial u_k}{\partial x_l} = i\varpi s_l u_k \tag{2.5}$$

Then equation 2.3 can be written as:

$$\frac{1}{\rho}\sum_{j=1}^{3}\sum_{l=1}^{3}\sum_{k=1}^{3} C_{ijkl} n_j n_l u_k = v^2 u_i \tag{2.6}$$

where $\vec{s} = \left(1/v\right)\vec{n}$, ie. $\vec{n}$ is a unit vector in the $\vec{s}$ direction.

This is a form of eigenvalue equation $Au = v^2 u$, where A is a 3×3 matrix, u is the column vector containing the components of u, and v^2 is the eigenvalues (Krebes, 2001). In summation, it can be written in matrix form as:

$$\sum_{k=1}^{3} A_{ik} u_k = v^2 u_i \tag{2.7}$$

where $A_{ik} = \frac{1}{\rho}\sum_{j-1}^{3}\sum_{l=1}^{3} C_{ijkl} n_j n_l$, $i,k = 1, 2, 3$

For isotropic media, matrix A can be obtained by substituting the formula for the stiffness tensor C_{ijkl} for anisotropic media into the formula for A_{ik} above. Solving the eigenvalue equation yields the eigenvalue $v^2 = \{\alpha^2, \beta^2, \beta^2\}$, i.e., the P, SV, and SH wave speeds in an isotropic medium. The eigenvector gives the direction of motion for P and S waves (parallel and perpendicular to the direction of wave propagation, respectively).

For VTI medium, three sets of eigenvalues and eigenvectors are obtained, corresponding to the P, SV, and SH waves. However, the VTI eigenvectors, which gives the direction of particle displacement, are no longer parallel and perpendicular to the direction of wave propagation for P and SV waves, respectively. So, these waves are not "pure" P and SV waves, but *quasi-P* (qP) and *quasi-SV* (qSV) waves.

Daley and Hron (1977) gave a clear derivation of the directional-dependent phase velocities:

$$\rho v_P^2(\theta) = \frac{1}{2}\left[C_{33} + C_{44} + \left(C_{11} - C_{33}\right)\sin^2\theta + D(\theta)\right] \tag{2.8-a}$$

$$\rho v_{SV}^2(\theta) = \frac{1}{2}\left[C_{33} + C_{44} + \left(C_{11} - C_{33}\right)\sin^2\theta - D(\theta)\right] \tag{2.8-b}$$

$$\rho v_{SH}^2(\theta) = C_{66}\sin^2\theta + C_{44}\cos^2\theta \tag{2.8-c}$$

Where ρ is density, and θ is the phase angle which refers the angle between the wavefront normal and the vertical axis.

$$\begin{aligned} D(\theta) = \{ &(C_{33} - C_{44})^2 + 2\left[2(C_{13} + C_{44})^2 - (C_{33} - C_{44})(C_{11} + C_{33} - 2C_{44})\right]\sin^2\theta + \\ &\left[(C_{11} + C_{33} - 2C_{44})^2 - 4(C_{13} + C_{44})^2\sin^4\theta \right\}^{1/2} \end{aligned} \tag{2.9}$$

Equations 2.8-a, 2.8-b and 2.8-c give the speeds of qP and qSV and qSH waves as a function of phase angle, respectively. When the waves travel in the vertical $\left(\theta = 0^o\right)$ and horizontal direction $\left(\theta = 90^o\right)$, the qP wave phase velocities reduce to:

$$v_{qP}\left(0^o\right) = \alpha_0 = \sqrt{C_{33}/\rho} = \sqrt{(\lambda''+2\mu)/\rho} \tag{2.10-a}$$

$$v_{qP}\left(90^o\right) = \alpha_{90} = \sqrt{C_{11}/\rho} = \sqrt{(\lambda+2\mu)/\rho} \tag{2.10-b}$$

The SV wave speeds in vertical and horizontal direction then reduce to:

$$v_{qSV}\left(0^o\right) = \beta_0 = \sqrt{C_{44}/\rho} = \sqrt{\mu'/\rho} \tag{2.11-a}$$

$$v_{qSV}\left(90^o\right) = \beta_{90} = \sqrt{C_{44}/\rho} = \sqrt{\mu'/\rho} \tag{2.11-b}$$

For q-SH waves, we obtain,

$$v_{qSH}\left(0^o\right) = \sqrt{C_{44}/\rho} = \sqrt{\mu'/\rho} \tag{2.12-a}$$

$$v_{qSH}\left(90^o\right) = \sqrt{C_{66}/\rho} = \sqrt{\mu/\rho} \tag{2.12-b}$$

For simplification, we will use P instead of qP wave, and SV instead of qSV in the following contents of this thesis.

2.2.5 Definition of anisotropy parameters

The equations above have been simplified by Thomsen (1986) for practical application, using three anisotropy parameters ε, δ and γ, which are defined as:

$$\varepsilon = \frac{C_{11} - C_{33}}{2C_{33}} \tag{2.13-a}$$

$$\delta = \frac{\left(C_{13} + C_{44}\right)^2 - \left(C_{33} - C_{44}\right)^2}{2C_{33}\left(C_{33} - C_{44}\right)} \tag{2.13-b}$$

$$\gamma = \frac{C_{66} - C_{44}}{2C_{44}} \tag{2.13-c}$$

These three parameters are non-dimensional and they reduce to zeros for isotropic medium. In formations where these combinations are much less than one, these formations are referred as ‘weak anisotropy’. These combinations are unique because the seismic velocities may be rewritten more compactly using them. Thomsen (1986) gave his definition of the anisotropy parameters connected with the velocities rather than the elastic components. They have become the conventional anisotropies used to characterize polar anisotropic formations in geophysical contexts.

ε is used to describe the fractional difference between vertical and horizontal P velocities according to equation 2.10-a and 2.10-b

$$\varepsilon = \frac{v_{qP}\left(90^0\right) - v_P(0^0)}{v_P\left(0^0\right)} = \frac{v_P\left(90^0\right) - \alpha_0}{\alpha_0} \tag{2.14-a}$$

where $\alpha_0 = v_{qP}\left(0^0\right)$.

According to equation 2.12-a and 2.12-b, γ, which corresponds to the conventional meaning of "SH anisotropy" is expressed by

$$\gamma = \frac{v_{SH}(90^0) - v_{SH}\left(0^0\right)}{v_{SH}\left(0^0\right)} = \frac{v_{SH}\left(90^0\right) - \beta_0}{\beta_0} \tag{2.14-b}$$

where $\beta_0 \equiv v_{SH}\left(0^0\right) = v_{qSV}\left(0^0\right)$.

Thomsen (1986) discussed the velocities in weak anisotropy, and defined δ as:

$$\delta = 4\left[\frac{v_P\left(45^0\right)}{\alpha_0} - 1\right] - \varepsilon \tag{2.14-c}$$

Berryman (1979) and Helbig (1979) show that if anisotropy is caused by fine layering of isotropic materials, then strictly ε > δ.

Thomsen (1986) showed there is no connection between the two anisotropy parameters δ and ε.

2.3 P-SV waves reflection and transmission coefficients

When a plane wave reaches a flat boundary, some of its energy is reflected by the boundary and some of its energy is transmitted through the boundary. In this section, we will calculate the reflection and transmission coefficients at non-normal incidence. Before discussing the anisotropic case, we need to examine the isotropic case first.

Figure 2.1 shows an incident P wave impinging non-normally upon a flat interface, which separates the two elastic media, I and II, at $z = 0$. The P-wave incidence is what interests us the most and will be discussed specifically here.

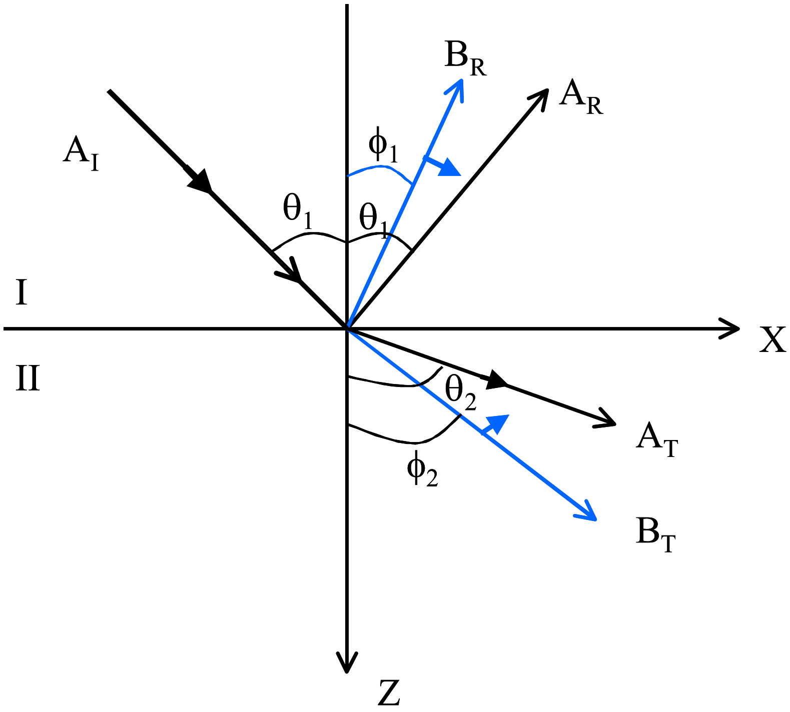

Figure 2.1 Reflection and Transmission of an incident plane P wave. A_I, A_R and A_T are the amplitudes of the P waves, and B_R, B_T are the amplitudes of SV waves. The boldface arrows defined the positive direction of particle motion.

There is an assumption that the incident wave is propagating in the xz plane. For a P or SV wave, it will cause the particles of the medium to move in the xz plane, and there will be no y component of particle motion (Crampin, 1985). This means that the reflected and transmitted waves will also be in xz plane. Similarly, for the incident SH wave, the particle motion will be in the y direction, which will produce the reflected and transmitted wave particle motion in the y direction only. So, an incident P or SV wave will generate both P and SV reflected and transmitted wave, but no SH waves. An incident SH wave will generate reflected and transmitted SH wave only.

2.3.1 Boundary condition equations (Zoeppritz equations)

To obtain the reflection and transmission coefficients, we must solve the equations describing the boundary conditions. There are two boundary condition equations which must be satisfied (Krebes, 2001). The first states that the displacement on one side of the interface must match the displacement on the other side. So the normal component of displacement u_z must be continuous across the interface, which can guarantee that wave motion will cause no normal separation of rock layers to occur. The boundary condition for tangential components u_X and u_Y states, that the wave motion will not cause slippage of one rock layer across the other along the boundary. Those are physically reasonable requirements. The other boundary condition states that the normal stress component σ_{ZZ}, and the tangential stress σ_{XZ} and σ_{YZ}, are continuous across the boundary, which means that there are no unbalanced stresses at the interface.

The six boundary equations can be separated into two groups: four of the equations, i.e., the ones for u_X, u_Z, σ_{XZ} and σ_{ZZ} apply to the P-SV case, and the remaining two, u_Y and σ_{YZ}, apply to the SH case.

In this thesis, only P-wave incidence with P- and SV-wave reflection is discussed. The SH wave incidence and reflection will not be considered.

Four P-SV equations can be solved for the relative amplitudes of the four reflected and transmitted P and SV waves to get the reflection and transmission coefficients. As shown in Figure 2.1, the Snell's law of reflection and transmission is expressed as:

$$p = \frac{\sin\theta_1}{\alpha_1} = \frac{\sin\theta_2}{\alpha_2} = \frac{\sin\phi_1}{\beta_1} = \frac{\sin\phi_2}{\beta_2} \tag{2.15}$$

where α_1, α_2 are the P wave velocities in medium I and II, respectively, and β_1, β_2 are SV wave velocities in medium I and II, respectively. Here, the angle of incidence is equal to the angle of the reflection for same wave type.

The boundary equations, which are also known as Zoeppritz equations, are given below. The displacement boundary equations for u_X and u_Z are:

$$(A_I + A_R)\sin\theta_1 + B_R\cos\phi_1 = A_T\sin\theta_2 + B_T\cos\phi_2 \tag{2.16-a}$$

$$(A_I - A_R)\cos\theta_1 + B_R\sin\phi_1 = A_T\cos\theta_2 - B_T\sin\phi_2 \tag{2.16-b}$$

The stress boundary equations for σ_{XZ} and σ_{ZZ} are expressed as:

$$2\rho\beta_1^2 p(A_I - A_R)\cos\theta_1 - \rho_1\beta_1\left(1 - 2\beta_1^2 p^2\right)B_R = 2\rho_2\beta_2^2 pA_T\cos\theta_2 + \rho_2\beta_2\left(1 - 2\beta_2^2 p^2\right)B_T$$

(2.16-c)

$$\rho_1\alpha_1\left(1 - 2\beta_1^2 p_2^2\right)(A_I + A_R) - 2\rho_1\beta_1^2 pB_R\cos\phi_1 = \rho_2\alpha_2\left(1 - 2\beta_2^2 p^2\right)A_T - 2\rho_2\beta_2^2 pB_T\cos\phi_2$$

(2.16-d)

There are four unknowns within these four linear equations (A_I is unknown), and we solve the equations for relative amplitudes to obtain the reflection and transmission coefficients as following:

The P-P reflection coefficient is $R_P = \frac{A_R}{A_I}$.

The P-SV reflection coefficient is $R_{SV} = \frac{B_R}{A_I}$.

The P-P transmission coefficient is $T_P = \frac{A_T}{A_I}$.

The P-SV transmission coefficient is $T_{SV} = \frac{B_T}{A_I}$.

Aki and Richards (1980) showed the approximate form of P-S reflectivity as:

$$R_{PSV} = -k\left[(1+\delta)\frac{\Delta\rho}{\rho} + 2\delta\frac{\Delta V_S}{\beta}\right] \tag{2.17}$$

where $k = (\gamma \tan\varphi)/2$,

$$\delta = -2\frac{\sin^2\theta}{\gamma^2} + 2\frac{\cos\theta\cos\varphi}{\gamma} \tag{2.18}$$

$$\gamma = \alpha/\beta \tag{2.19}$$

$$\Delta\rho = \rho_{lower} - \rho_{upper} \tag{2.20}$$

$$\rho = \frac{1}{2}(\rho_{lower} + \rho_{upper}) \tag{2.21}$$

$$\Delta V_S = V_{S\,lower} - V_{S\,upper} \tag{2.22}$$

$$\beta = \frac{1}{2}(V_{S\,lower} + V_{S\,upper}) \tag{2.23}$$

$$\alpha = \frac{1}{2}\left(V_{P\,lower} + V_{P\ upper}\right) \tag{2.24}$$

$$\theta = \frac{1}{2}\left(\theta_1 + \theta_2\right) \tag{2.25}$$

$$\varphi = \frac{1}{2}\left(\varphi_1 + \varphi_2\right) \tag{2.26}$$

Equation (2.17) is a good approximation when media 1 and media 2 have similar elastic constants.

2.3.2 *Phase angle vs. ray angle, phase velocity vs. group velocity*

Thomsen (1986) showed that the energy does not travel along the direction that the ray path travels in the anisotropic case because the wavefront is not spherical (Figure 3.2).

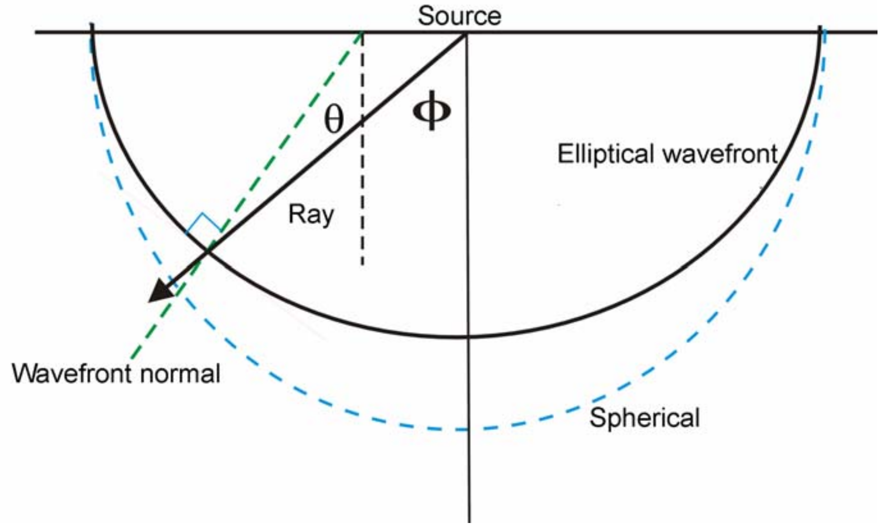

Figure 2.2 Graph of the definitions of phase angle, θ, and group (ray) angle, ϕ (Thomsen, 1986).

In anisotropic media, the wavefront-normal angle is called the phase angle, which is represented as θ, while the angle from the source point to the wavefront is called the ray angle, which is represented by ϕ. The wavefront-normal velocity is called the phase velocity, and the energy traveling velocity is called the group velocity. These two are different, not only in their magnitude, but also in direction. In anisotropic media, it is the phase angles and phase velocity which obey Snell's law.

2.3.3 P and SV wave reflection and transmission calculation in VTI media

As we have discussed before, the velocity in anisotropic medium is angle-dependent. So the P and SV wave velocity α and β in section 2.3.1 have to be substituted by the angle-dependent velocity calculated by equation (2.8).

A Matlab code for computing reflection and transmission coefficients for solids with any type of anisotropy was developed by Dr. Krebes using equations (2.7) derived above, with ray parameter p as input. The output parameters calculated include the angle-variant phase velocities, ray velocities, and the reflection and transmission coefficients. When this program is used to do calculation for isotropic media, the anisotropic parameters have to be revised to become slightly anisotropic, to eliminate the degeneracy.

2.4 Model examples and results

Two VTI models were created, and the reflection and transmission coefficients on the interface were calculated. The corresponding coefficients for isotropic case were also calculated for comparison. In the first model, velocity and density in layer I are greater than that in layer II, and the relationship is opposite in the second model.

We notice that for a phase angle within –90 to 90 degrees, the related ray angle may not be within this range. The ray angle outside of this range has no physical meanings. Only the incidents and reflected rays with physical meaning are displayed.

2.4.1 Model-A

A two-layer model was created with the properties shown in Table 2.1. In this model, the velocity unit is km/s, and the density unit is g/cm^3. The impedance (the products of density and velocity) in layer I is less than that of layer II.

Table 2.1 Properties table of model-A

Property	$V_P(0^o)$	$V_{SV}(0^o)$	Density	ε	δ	γ
Layer I	2.5	1.25	1.4	0.20	0.20	0.1
Layer II	4.0	2.0	2.0	1.e-5	1e-5	1.e-5

The P-P, and P-SV reflection coefficients, varying with different ray angles, are shown together with the isotropic curve for comparison as Figure 2.3 and Figure 2.4

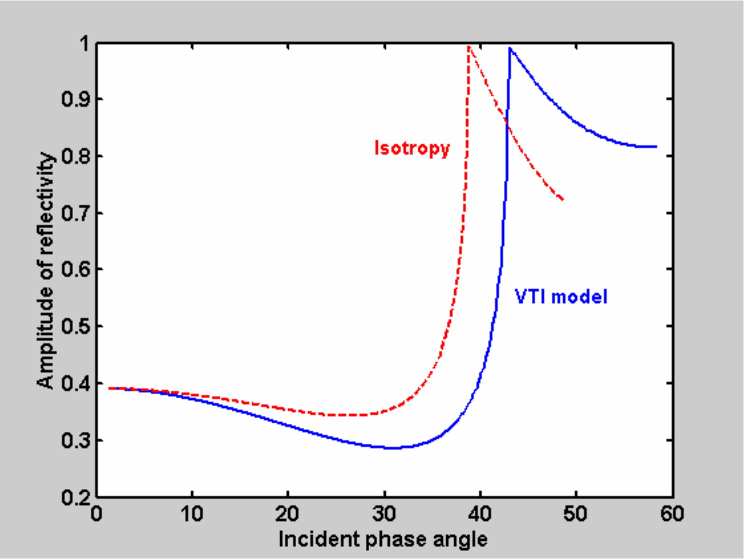

Figure 2.3 P-P reflection coefficients calculated from the mode-A defined as Table 2.1. The solid line represents the result obtained from the VTI case, and the dashed line refers to the isotropic case.

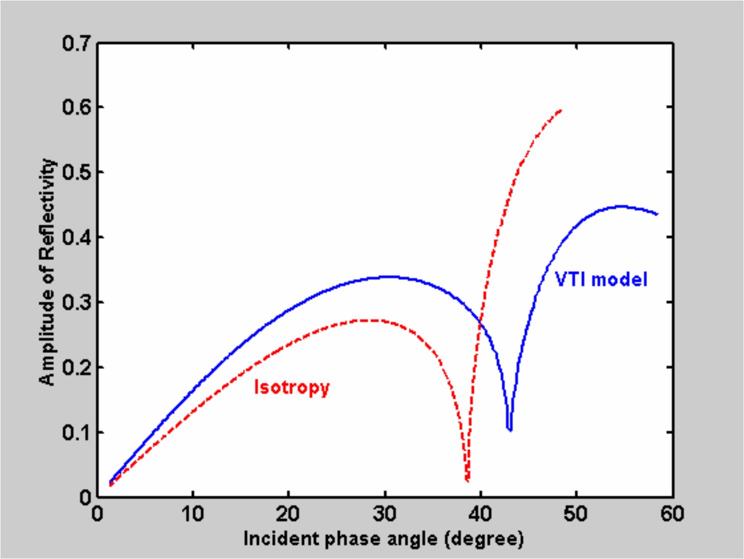

Figure 2.4 P-SV reflection coefficient variation with the incident ray angle in Model A. The solid line represents the VTI case and the dashed line represents the isotropic case.

In this model, there exists a critical angle due to the fact that the impedance in layer I is less than that of layer II. The critical angle in VTI case is greater than that in the isotropic case.

2.4.2 Model-B

Another model, model-B was created for further tests. Similar to model-A, the velocity unit is expressed in km/s, and the density is expressed in the unit of g/cm^3. The impedance of layer I is greater than that of layer II, so there won't be a critical angle in this model.

Table 2.2 Properties table of model-B

Property	V_P (0º)	V_{SV}(0º)	Density	ε	δ	γ
Layer I	6.0	3.0	2.5	0.20	0.20	0.1
Layer II	3.0	1.5	2.0	1.e-5	1e-5	1.e-5

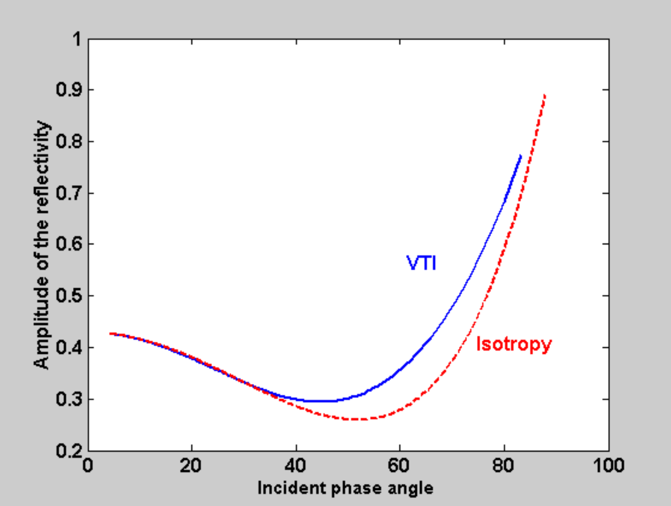

Figure 2.5 P-P reflection coefficient variation with the incident ray angles in model –B. The isotropic case is also shown for comparison.

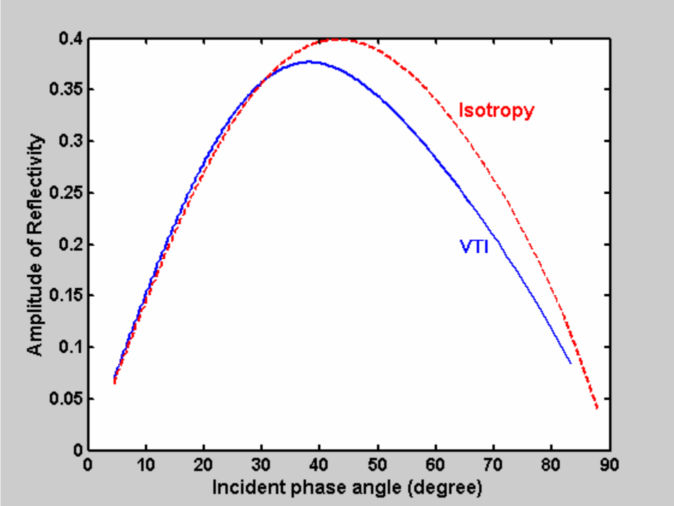

Figure 2.6 P-SV reflection coefficients variation with the incident ray angles. The dashed line shows the P-SV reflection on Model-B in isotropic case

2.5 Discussion

From lower impedance to higher impedance, the P-P reflectivity in VTI is smaller than that in isotropic case for angles below 43°, but the P-SV reflectivity amplitude is larger than that in isotropic case (Model-A) for angles below 40°. The critical angle in VTI case is greater than that angle in isotropic case.

From higher impedance to lower impedance, the P-P reflectivity in VTI model is larger than that in isotropic case (Model -B) for angles below 35°.

Chapter three:

P-S Conversion Point Mapping in VTI Model

3.1 Introduction

Converted waves are being more and more widely used in seismic exploration, for they can provide high-quality images where conventional images are poor (Stewart et al., 1999). It has been proven that the location of the conversion point is critical to P-S seismic survey design (Lawton and Cary, 2000). Also the P-S conversion point location is of great importance to P-S data binning and Common Conversion Point (CCP) stacking and NMO corrections. In isotropic media, the location of the P-S conversion point can be calculated by using the Snell's law. It then can be simplified by using asymptotic binning (Tessmer and Behle, 1988). However, it is well known that the earth's crust is inhomogeneous and anisotropic. Almost all conventional seismic surveys and processing procedures have not taken anisotropy into consideration. This isotropy assumption could lead to large errors in NMO correction, stacking and migration, which have been shown by many authors (e.g. Alkhalifah and Larner, 1994).

Anisotropy has less influence on P-waves than on S- (or converted) waves. In this anisotropic case, due to the difference between the group velocities and phase velocities and the difference between the ray angles and phase angles, there could be a difference in the P-S conversion point location between anisotropic and isotropic cases.

The most commonly considered anisotropic medium is the Vertical Transverse Isotropy (VTI) case. When the formation is shown to be VTI, the location of the conversion point will depart horizontally from that in an isotropic case, and it cannot be approximated by the isotropic case. Therefore, the horizontal position of the conversion point on the reflector has to be calculated specifically for VTI media. However, this requires knowledge of VP, VS, and anisotropy parameters. Otherwise, it will lead to problems in NMO correction and stacking which could cause traces that do not contain reflector energy to be summed, and those that do contain reflector energy not to be summed (Tessmer et al., 1990).

In this chapter, the P-S conversion point location will be mapped for a VTI medium. The displacement of the conversion point in the VTI model relative to its location in isotropic case will be calculated. The dependence of this displacement on the anisotropy parameters, the Vp/Vs ratio, and the offset/depth ratio will also be discussed.

3.1.1 P-S conversion point approximation in isotropic case

As discussed in Chapter One, in a single layer model, the conversion point location is determined by Snell's law, which is expressed by equation (1.1). This conversion point offset is dependent on the depth of the reflector and v_P/v_S in the overburden.

Tessmer and Behle (1988) gave a formula to calculate approximately the coordinate of the conversion point in a homogeneous and isotropic layer, which for a small incident angle (i.e. small offset/depth) such that $\tan\theta \cong \sin\theta$ for the angle of incidence, θ,

$$x_C = \frac{x}{1+\left({}^{v_S}\!/_{v_P}\right)} \tag{3.1}$$

Where x is the source-receiver offset, and x_C is the conversion point offset from the source.

Because the P-S velocity ratio v_P/v_S is always larger than 1, the up-going S-wave is closer to vertical than the down-going P-wave leg. Thus, the conversion point is closer to the receiver than is the midpoint.

3.1.2 Depth-variant conversion point position

Tessmer and Behle (1988) showed that in multi-layered strata, the actual P-S conversion point is not a constant offset from the source, but traces a trajectory that moves towards the receiver as the depth decreases (Figure 3.1). The conversion points moves towards the receiver when the offset/depth ratio increases. The asymptote of this trajectory, at large offset/depth is defined by equation (3.1).

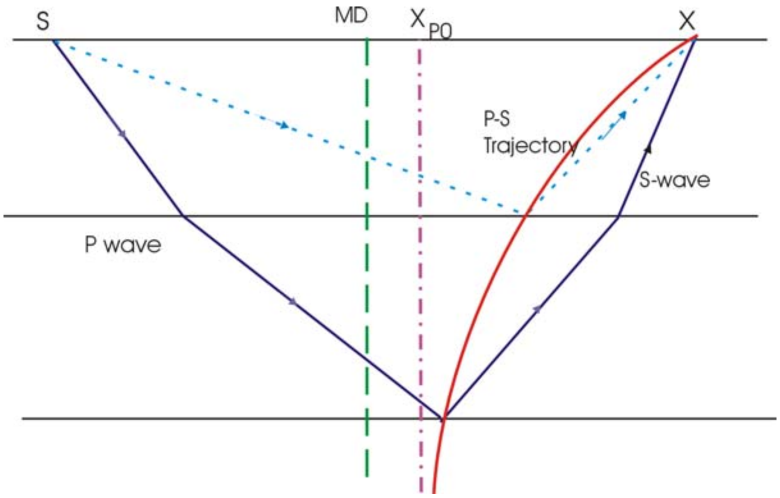

Figure 3.1. The conversion point traces a trajectory in the multi-layered model for a certain offset, instead of locating on a vertical axis (Stewart et al., 1999).

For larger offsets (or shallow depths), Tessmer and Behle (1988) expressed the trajectory equation in single layer explicitly as:

$$\left[\frac{x_C\left(x-x_C\right)}{z}\right]^2+\left[x_C^2-\frac{(2\gamma)^2}{\left(\gamma^2-1\right)}x\left(x_C-{}^{x}\!/_{2}\right)\right]=0 \tag{3.2}$$

where x is the source-receiver offset, and x_C is the conversion point offset, γ is the P-S velocity ratio.

3.2 Theory of conversion point mapping

As discussed in chapter two, Thomsen (1986) defined three parameters ε, δ and γ to characterize formation anisotropy. He also deduced the velocity equations, which are functions of the phase angle and the anisotropic parameters, and the relationship between the phase angle and the group angle.

The angle-dependent velocity can be calculated using the following formulae (Thomsen, 1986):

$$v_p^2(\theta)=\alpha_0^2\left[1+\varepsilon\sin^2\theta+D^*(\theta)\right] \tag{3.3-a}$$

$$v_{sv}^2(\theta)=\beta_0^2\left[1+\frac{\alpha_0^2}{\beta_0^2}\varepsilon\sin^2\theta-\frac{\alpha_0^2}{\beta_0^2}D^*(\theta)\right] \tag{3.3-b}$$

$$v_{SH}^2(\theta)=\beta_0^2\left[1+2\gamma\sin^2\theta\right] \tag{3.3-c}$$

with

$$D^*(\theta)=\frac{1}{2}\left(1-\frac{\beta_0^2}{\alpha_0^2}\right)\left\{\left[1+\frac{4\delta^*}{(1-\beta_0^2/\alpha_0^2)}\sin^2\theta\cos^2\theta+\frac{4(1-\beta_0^2/\alpha_0^2+\varepsilon)\varepsilon}{(1-\beta_0^2/\alpha_0^2)}\sin^4\theta\right]^{1/2}-1\right\} \tag{3.4}$$

where α_0, β_0 is the P-wave velocity and S-wave velocity along the vertical axis, respectively, for VTI medium.

The ray angle, ϕ, can be expressed as a function of phase angle, θ, given by the following equation:

$$\tan[\varphi(\theta)] = \frac{(\tan\theta + \frac{1}{v}\frac{dv}{d\theta})}{(1 - \frac{\tan\theta}{v}\frac{dv}{d\theta})} \tag{3.5}$$

The group velocity at ray angle ϕ, $V(\phi)$, is related to phase velocities at angle θ by:

$$V^2[\varphi(\theta)] = v^2(\theta) + \left(\frac{dv}{d\theta}\right)^2 \tag{3.6}$$

Using the Taylor-series expansion for small ε, δ^* and γ, Thomsen (1986) derived the linear approximation for weak anisotropy:

$$D^*(\theta) \approx \frac{\delta^*}{\left(1 - \beta_0^2 / \alpha_0^2\right)} \sin^2\theta \cos^2\theta + \varepsilon \sin^4\theta \tag{3.7}$$

By substituting the equation (3.7) into the equations (3.3-a), (3.3-b), (3.3-c), respectively, the following linear approximation of the velocities are derived as:

$$v_P(\theta) = \alpha_0 \left(1 + \delta \sin^2\theta \cos^2\theta + \varepsilon \sin^4\theta\right) \tag{3.8-a}$$

$$v_{SV}(\theta) = \beta_0 \left(1 + \frac{\alpha_0^2}{\beta_0^2}(\varepsilon - \delta)\sin^2\theta \cos^2\theta\right) \tag{3.8-b}$$

$$v_{SH}(\theta) = \beta_0 \left(1 + \gamma \sin^2\theta\right) \tag{3.8-c}$$

Then the δ^* is replaced with another parameter, δ, using the relationship:

$$\delta = \frac{1}{2}\left[\varepsilon + \frac{\delta^*}{\left(1 - \beta_0^2/\alpha_0^2\right)}\right] \tag{3.9}$$

The relationship between the group angle, ϕ, and phase angle,θ, in the linear approximation form can be expressed as:

$$\tan\phi = \tan\theta\left[1 + \frac{1}{\sin\theta\cos\theta}\frac{1}{v(\theta)}\frac{dv}{d\theta}\right] \tag{3.10}$$

For P waves, substituting equation (3.8-a) into equation (3.10) leads to

$$\tan\phi_P = \tan\theta_P\left[1 + 2\delta + 4(\varepsilon - \delta)\sin^2\theta_P\right] \tag{3.11-a}$$

Similarly, for SV-wave and SH-waves,

$$\tan\phi_{SV} = \tan\theta_{Sv}\left[1 + 2\frac{\alpha_0^2}{\beta_0^2}(\varepsilon - \delta)\left(1 - 2\sin^2\theta_{SV}\right)\right] \tag{3.11-b}$$

$$\tan\phi_{SH} = \tan\theta_{SH}\left(1 + 2\gamma\right) \tag{3.11-c}$$

In this chapter, these equations are the theoretical bases for the calculation of the horizontal coordinate of the conversion point for given offset/depth ratio, anisotropy parameters, and the velocity ratio γ.

3.3 Methodology

Using Thomsen's linear-approximation equations, we developed an algorithm to calculate the horizontal distance between the theoretical conversion points in a VTI medium and in an isotropic medium for the same offset, which is shown in Figure 3.2. Figure 3.3 displays the relationship between the angles and offsets in the algorithm flow. In Figure 3.3, X refers the source-receiver offset, while X_{P1} and X_{P0} refer to the P-S conversion point offset from the source in the VTI and isotropic cases, respectively.

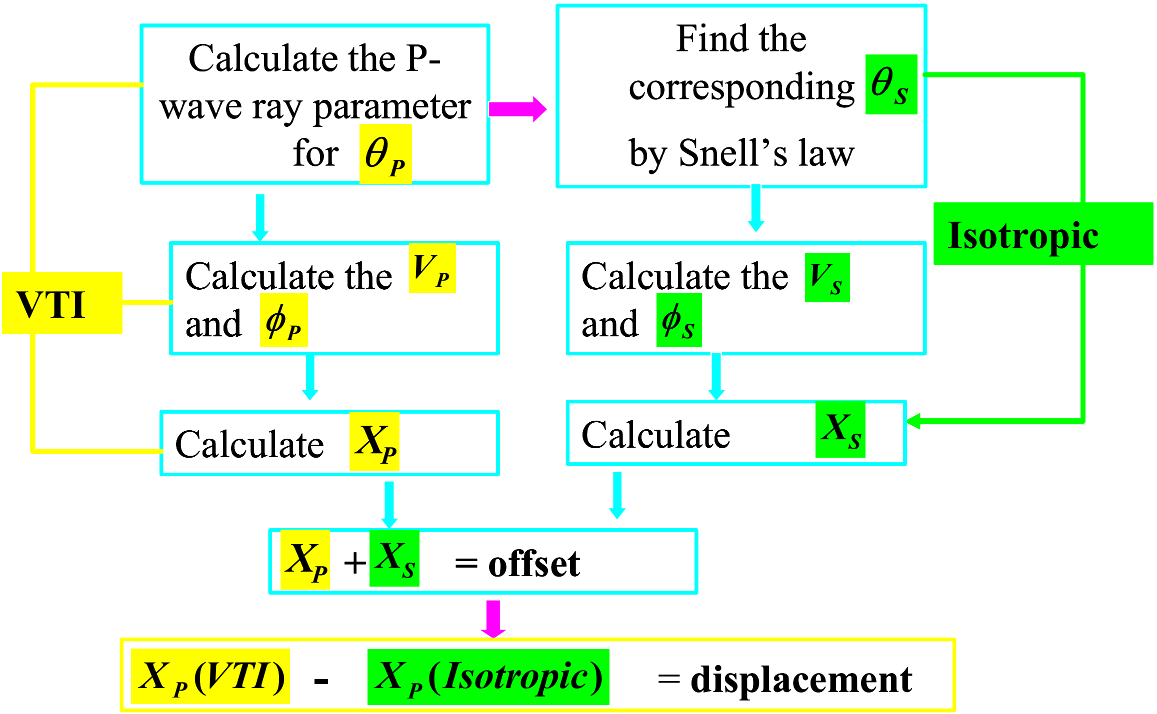

Figure 3.2 Flow chart of this algorithm developed to calculate the displacement of the conversion point.

Firstly, the method computes a fan of P-wave phase angles θ_P (such as from 0 to 60 degrees, with a step of 0.25 degrees), then the corresponding P-wave phase velocity at each angle, $v_P(\theta)$ by using equation (3.3-a). Then the P-wave ray parameter, p_P, for each angle by using equation (2.15) is calculated.

According to Snell's law, the SV-wave ray parameter p_{SV} has to be equal to the p_p calculated. A series of SV-wave phase velocities, $v_{SV}(\theta)$, are calculated using equation (3.3-b) for a number of SV wave phase angle (such as from 0 to 60 degrees, with interval of 0.25 degree). Then the p_S will be obtained and can be matched with the p_p.

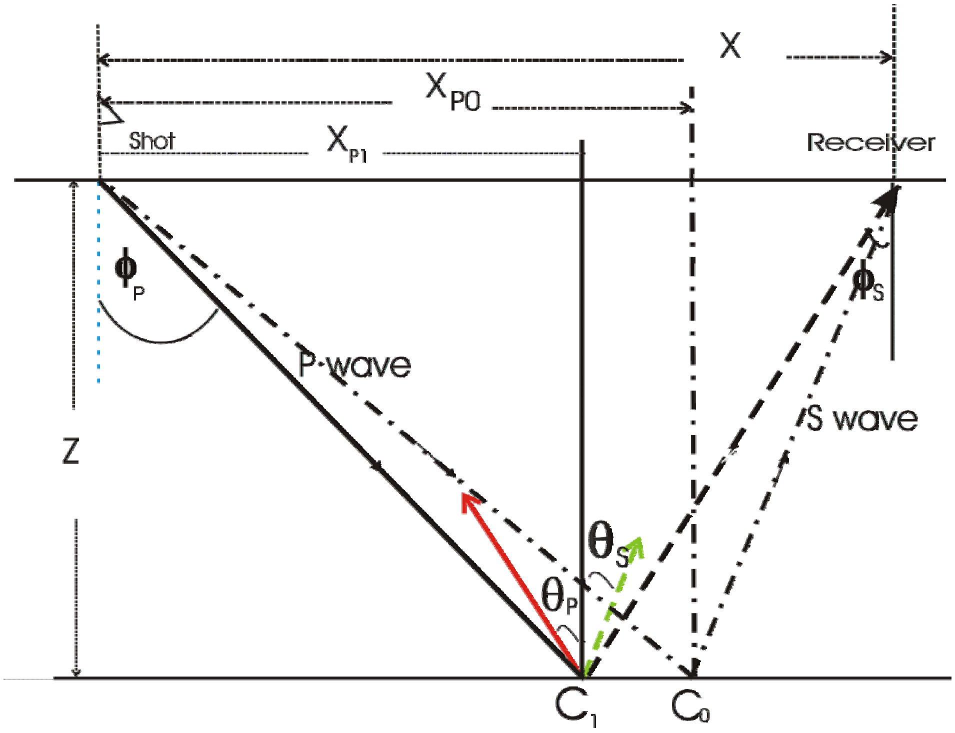

Figure 3.3 The chart showing the angles and offsets included in the algorithm. C_1 refers the conversion point location in VTI case, and C_0 refers the conversion point in isotropic case.

For each P-wave phase angle, and for given values of ε and δ, the group angle, ϕ_P, is first calculated using Thomsen's exact equation (3.10). The horizontal coordinate of the conversion point X_{P1} is calculated by using the group angle and the thickness of the VTI medium in the formula $X_{P1} = z * \tan\phi_P$.

For each S-wave phase angle that matches the P wave incident angle, its group angle ϕ_S is calculated by using equation (3.10). Then the distance from the conversion point to the receiver X_{S1}, shown in Figure 3.3, is calculated from $X_{S1} = z * \tan\phi_{SV}$, which is the distance between the conversion point and the receiver.

A series of offsets X for each phase angle θ_P can be obtained by adding these two distances together: the distance from the conversion point to the source X_{P1}, and the distance from the conversion point to the receiver X_{S1}. Thus, the corresponding offset-to-depth ratio can be obtained.

Then given the offset X in an isotropic medium, the conversion-point offset X_{P0}, can be determined by Snell's law for different angles. The distance between the two conversion points ($X_{P1} - X_{P0}$), which is the displacement of the conversion point in VTI media from that in isotropic case for same offset, is then obtained.

The linear approximation forms of ray angle, i.e., equation (3.11-a, 3.11-b, 3.11-c), and phase velocities, i.e., equations (3.8-a, 3.8-b, 3.8-c) can also be applied by replacing the exact equations, with the linear approximations.

3.4 Examples and results

3.4.1 Results obtained from exact equations and linear approximation

For the VTI model with ε = 0.10 and δ = 0.05, the displacement of the conversion point, relative to the isotropic case was calculated using Thomsen's exact equations for phase velocities and ray angles and linear-approximation equations, respectively. The same procedures were conducted for δ = 0.10 and δ = 0.2. The thickness of the model is 1032 m, which is set to keep the same as a scaled physical model used in Chapter 5. Figure 3.4(a) and Figure 3.4(b) display the variation in displacement of the conversion point with the variation in the offset to depth ratio.

In these two figures, the positive value represents the conversion point displacement towards receiver, while negative value represents the conversion point displacement towards to the source, relative to the conversion point locations in the isotropic case.

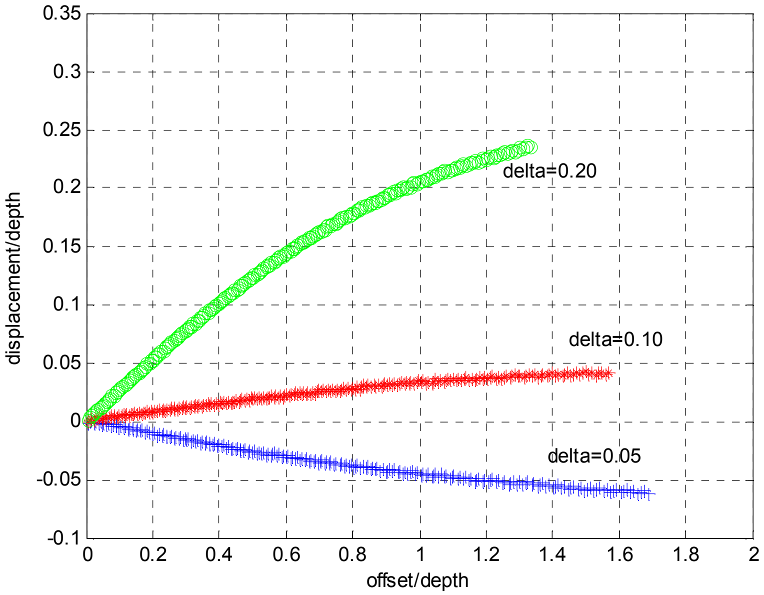

Figure 3.4 (a) Variation of the displacement of the conversion point with the variation of the offset to depth ratio, computed from Thomsen's linear approximation of phase velocities equation for different value of delta.

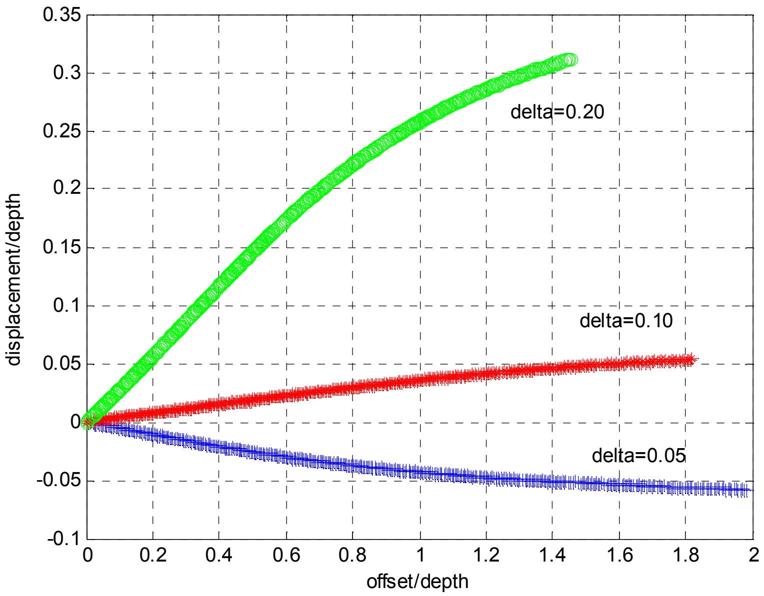

Figure. 3.4 (b) Variation of the displacement of the conversion point with the variation of the offset to depth ratio, computed from Thomsen's exact equations for phase velocities.

3.4.2 Conversion point scatter dependence on ε and δ

A series of 3-D curved surfaces, from Figure 3.5(a) to Figure 3.5(f), are plotted to display the variation of the displacement of the conversion point with offset-to-depth ratio, and the anisotropy parameter ε. These results are obtained from the exact equations for ray velocities and ray angles discussed earlier in this chapter.

An example of the ray path of the P-S wave in the VTI model with ε = 0.10, δ = -0.05 and δ = 0.20, respectively, and the ray path in isotropic case, are also plotted to show the displacement of the conversion point (Figure 3.6). In this case, the distance of these two conversion points in the VTI model with different values of δ can be as large as 480 m.

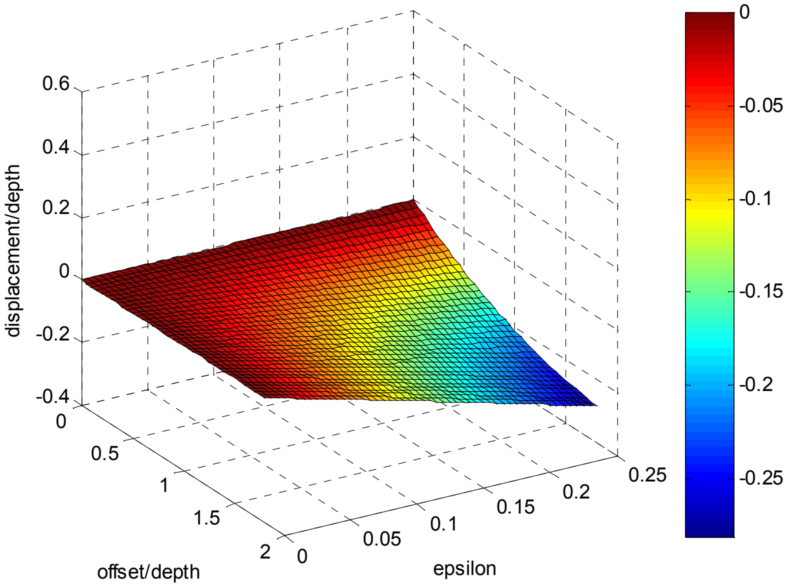

Figure 3.5 (a) Surface showing the variation of displacement/depth of the conversion point in VTI media relative to its location in the isotropic case, with the variation of the offset-to-depth ratio and ε. Here, δ = 0.25 ε.

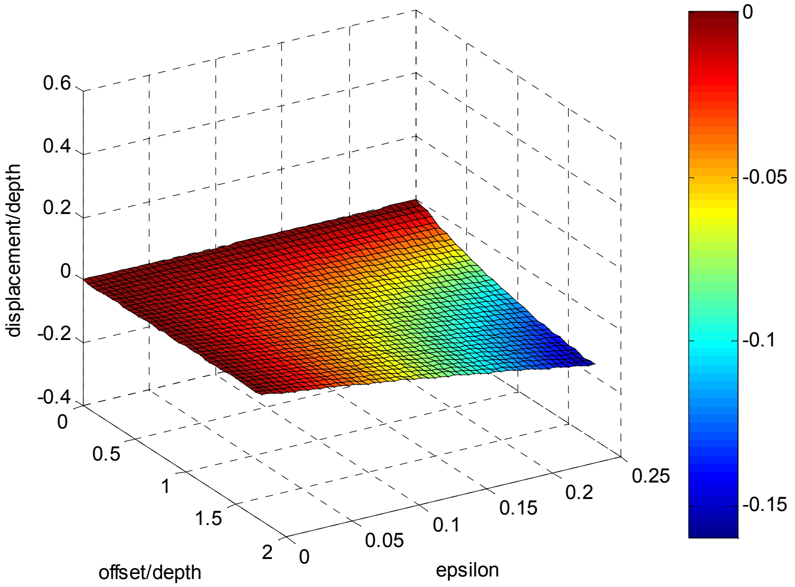

Figure 3.5 (b) Surface showing the variation of displacement/depth of the conversion point in VTI media relative to its location in the isotropic case, with the variation of the offset-to-depth ratio and ε. Here, δ = 0.50 ε.

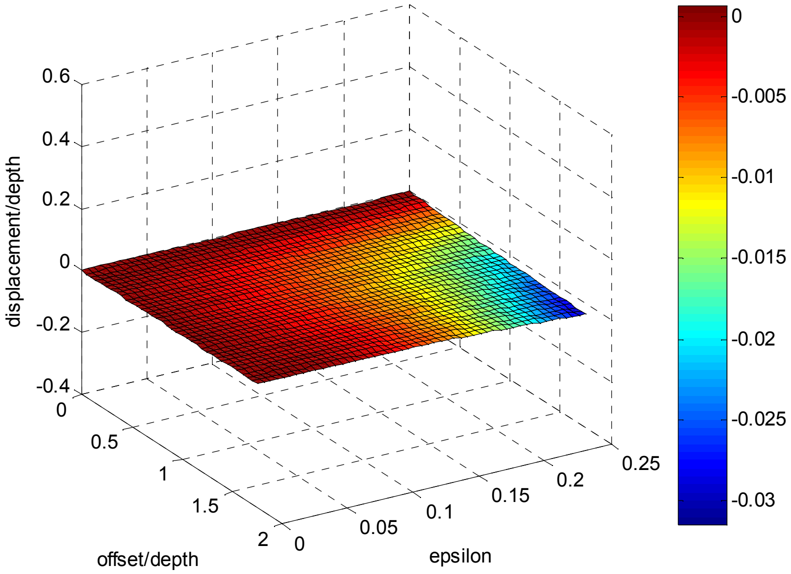

Figure 3.5 (c) Surface showing the variation of displacement/depth of the conversion point in VTI media relative to its location in the isotropic case, with the variation of the offset-to-depth ratio and ε. Here, δ = 0.75 ε.

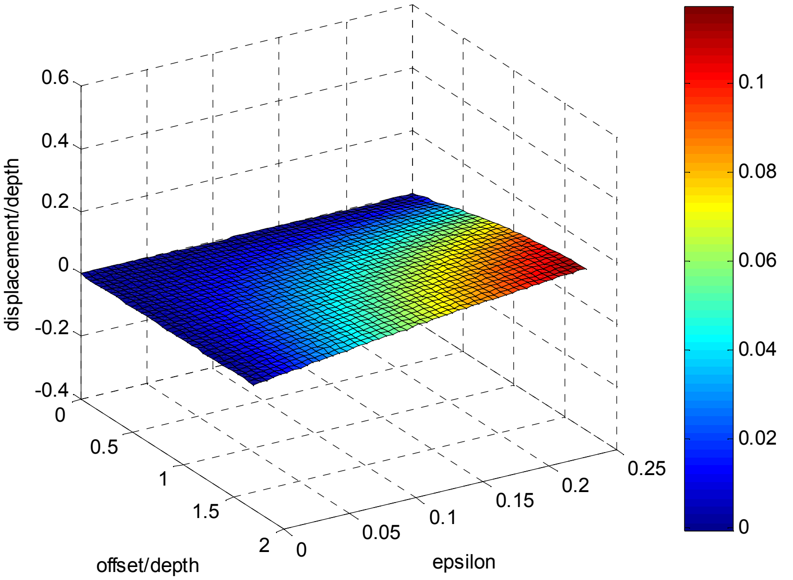

Figure 3.5 (d) Surface showing the variation of displacement/depth of the conversion point in VTI media relative to its location in the isotropic case, with the variation of the offset-to-depth ratio and ε. Here, δ = ε, "elliptical" VTI.

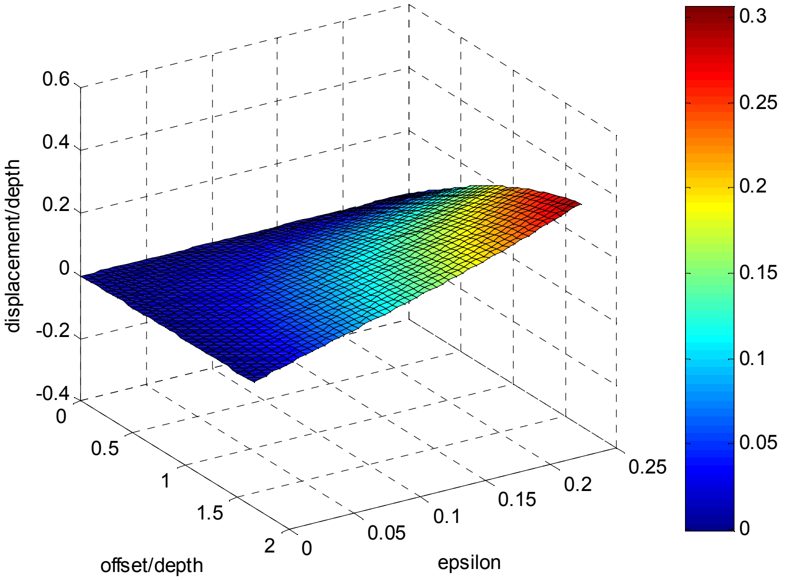

Figure 3.5 (e) Surface showing the variation of the displacement/depth of the conversion point in VTI media relative to its location in the isotropic case, with the variation of the offset-to-depth ratio and ε. Here, δ = 1.25 ε.

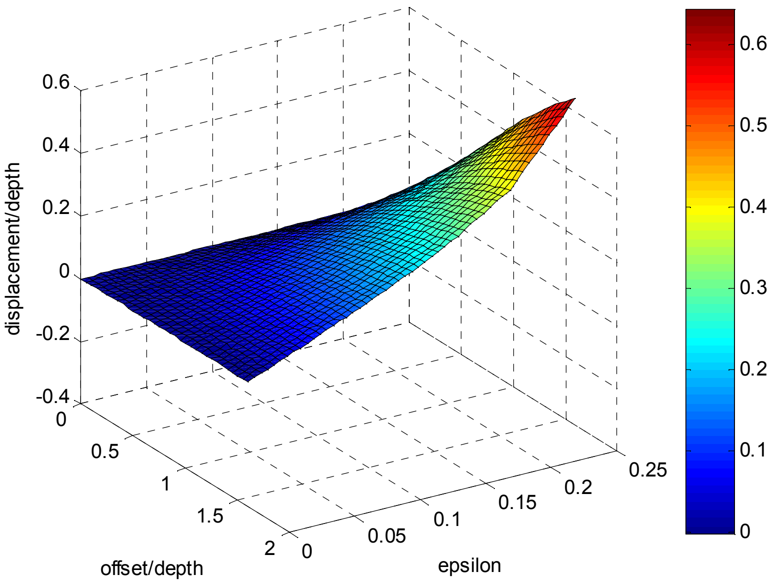

Figure 3.5 (f) Surface showing the variation of the displacement-to-depth ratio of the conversion point in VTI media relative to its location in the isotropic case, with the variation of the offset-to-depth ratio and ε. Here, δ = 1.5 ε.

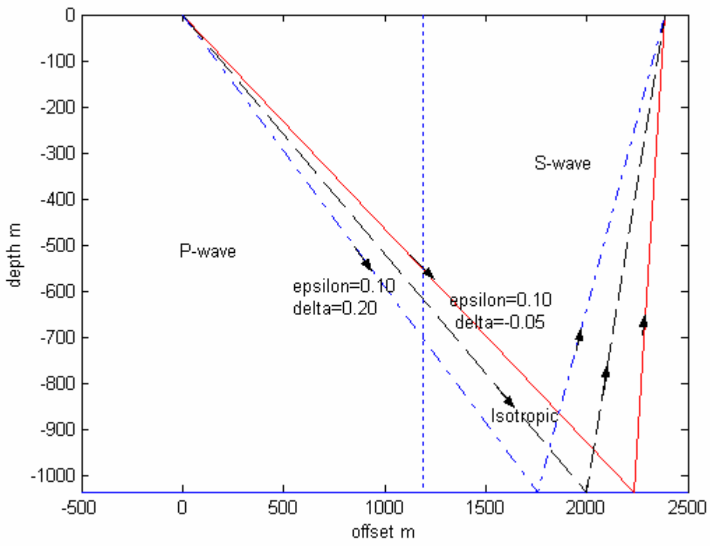

Figure 3.6 Example of P-S raypath in VTI model with ε = 0.10, δ = -0.05 and δ = 0.20.

3.4.3 Conversion point scatter dependence on V_P / V_S

We have known that the velocity ratio will have influence on P-S conversion point position in isotropic media. How does the velocity ratio affect the P-S conversion point position in VTI case? The displacement of conversion point from the isotropic case varying with different velocity ratio, were calculated on two models with different anisotropy parameters. The results are shown in Figure 3.7 (a) and Figure 3.7(b).

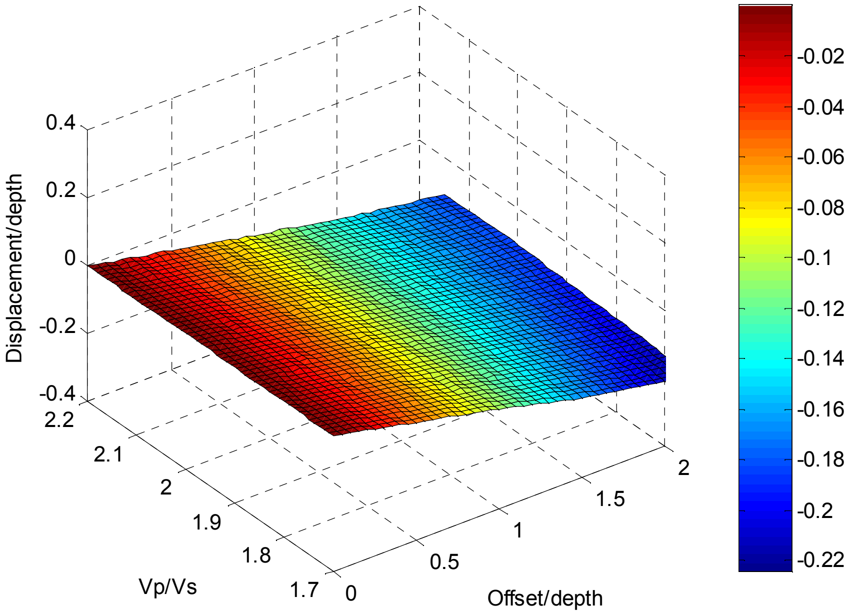

Figure 3.7(a) Displacement/offset variation with Vp/Vs for the model with ε = 0.20, δ = 0.10. The positive displacement/offset means that the conversion point is located towards the receiver compared with the isotropic case.

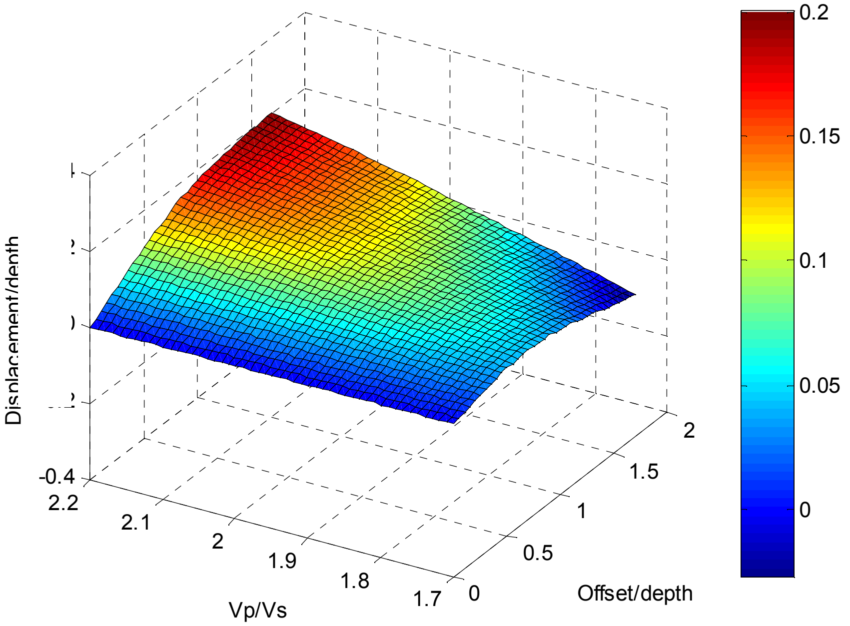

Figure 3.7(b) The displacement/offset varies with Vp/Vs in a model with $\varepsilon = 0.20$, $\delta = 0.30$. The positive displacement means that the conversion point is located towards the receiver related to the isotropic case.

3.5 Discussion

Results from the analysis show that the conversion point in the anisotropic case can be very different from that in the isotropic case. The horizontal displacement of the conversion point in VTI media from that in isotropic media is dependent on offset-to-depth ratio, and anisotropy parameters (Figure 3.5(a) to Figure 3.5(f)). It increases with the increasing offset-to-depth ratio and anisotropic parameter ε.

When $\delta < \varepsilon$, for the same offset, the conversion point moves towards the source in VTI media relative to that in the isotropic case (Figures 3.5 (a), Figure3.5 (b), Figure 3.5 (c)). When $\delta \geq \varepsilon$ for same offset, the conversion point moves towards the receiver (Figures

3.5(d), Figure 3.5(e) and Figure 3.5(f)). Before this experiment was conducted, it had been assumed generally that the conversion point moves towards the source with increasing anisotropy.

It has been proven that in most sedimentary formations, the value of ε is generally larger than the value of δ (Thomsen, 1986). So, the conversion point moves towards the source in most cases of VTI media. The displacement of the conversion point cannot be ignored in formations with transversely isotropic characteristics. When the formation is shown to be anisotropic, the conversion point can't be approximated by the position found in the isotropic case.

The velocity ratio doesn't have a significant influence on the displacement of the conversion point for small offset/depth, but has significant influence on for large offset/depth, which can be seen from Figure 3.7(a) and Figure 3.7(b).

For small offset-to-depth ratios, there is no significant difference between the results obtained from Thomsen's exact equations for anisotropic velocities and ray-angle calculations, and the results from the linear-approximation equations. However, there is a large difference for offset-to-depth ratios greater than 1.5.

All our calculations are based on the assumption that the accuracy of measurement of the anisotropy parameters can be guaranteed.

Chapter four

Comparison of three P-SV conversion point mapping approaches in VTI media

4.1 Introduction of this chapter

In chapter three, the conversion point position in VTI media was mapped by using Thomsen's exact equations and through using linear approximations. The displacement of conversion point in VTI media from its location in isotropic case was calculated for varying anisotropy parameters, offset/depth, and V_P/V_S.

Thomsen (1999) also provided an approximation method for P-S converted wave ray mapping, which is called the effective velocity ratio method. In this method, the exact conversion point offset equation is expressed by using Taylor series. The influence of anisotropy and layering effect are all included in one special parameter, γ_{eff}. In this chapter, this method will be introduced and applied for P-S converted wave ray tracing. The result obtained from this method will be compared with the exact calculation.

Currently, there are several types of commercial software in use, which are developed for anisotropy raytracing, such as GXII, and NORSAR2D. Another object of this thesis is to test the efficiency of these tools in P-SV converted wave raytracing. In this chapter, NORSAr2D will be tested for P-SV converted wave ray tracing, and compared with the results obtained from Thomsen's equations.

4.2 The effective velocity ratio method

4.2.1 P-S conversion point calculation in isotropic media

The incident P-wave converts part of its energy to S-waves at interface. The upgoing S-wave travels more steeply than the downgoing P ray, because of Snell's law and the fact that $V_P/V_S > 1$. The offset of the conversion-point from the source is based on physical properties of the media, not on simple geometry.

For a single, homogeneous, isotropic layer, i.e., Figure 1.3, the exact conversion-point offset from the source can be expressed as (Thomsen, 1999):

$$\frac{x_C}{x} = \frac{V_P t_P(x)\sin\theta_P}{V_P t_P(x)\sin\theta_P + V_S t_S(x)\sin\theta_S} = \frac{1}{1+\dfrac{t_S(x)}{\gamma^2 t_P(x)}} \tag{4.1}$$

where t_P is the one-way oblique traveltime through the layer for the P-wave, t_S is the corresponding one-way S-wave time, V_P is P-wave velocity, and V_S is the shear-wave velocity.

At the limit when $z/x \to \infty$, which means the P- and S-wave ray paths are almost vertical, the ratio of traveltimes becomes $t_S/t_P \to t_{S0}/t_{P0} = V_P/V_S = \gamma$. So equation (4.1) is reduced to the Asymptotic Conversion Point (ACP) (Tessmer and Behle, 1988):

$$x_{C0} = x\frac{\gamma}{1+\gamma} \tag{4.2}$$

A Common Conversion Point (CCP) gather should be obtained by computation and depth-dependent sorting. However, it is common to bin the traces with a range of offsets from 0 to $X_{\max}$ with a common ACP. Thomsen (1999) proved that the smearing of the true conversion point should not be neglected. It is clear that the actual conversion point at finite z/x differs significantly from the shallow reflectors when $z/x \geq 1$, where considerable exploration interest for converted-waves lies.

4.2.2 *The effective velocity ratio (γ_{eff}) method in VTI media*

From the introduction, it is known that the ACP deviates from the true location of P-S conversion point, even in the homogeneous, isotropic layer. In chapter three, it was shown that anisotropy does affect the basic processing and interpretation steps for converted waves and anisotropy has to be taken into consideration for realistic problems. In this section, another method for converted wave ray tracing in VTI media will be introduced.

A Taylor expansion form as a function of x/z, was derived in order to compute the conversion point more efficiently. It is asymptotically correct at both limits ($x/z \to 0$ and $x/z \to \infty$) and varies smoothly in between them. This is expressed as (Thomsen, 1999):

$$\frac{x_c}{x} \approx C_0 + C_2 \frac{\left(x/z\right)^2}{\left(1 + C_3\left(x/z\right)^2\right)} \quad , \tag{4.3}$$

where the coefficients are $C_0 = \dfrac{\gamma}{1+\gamma}$; $C_2(\gamma) = \dfrac{\gamma}{2}\dfrac{(\gamma-1)}{(\gamma+1)^3}$; and $C_3 = \dfrac{C_2}{1-C_0}$.

In this method, the anisotropy effect is attributed to a parameter defined as effective velocity ratio. In a single-layer case, it can be expressed as:

$$\gamma_{eff} = \frac{\gamma_2^2}{\gamma_0} = \gamma_0 \frac{(1+2\delta)}{(1+2\sigma)} \tag{4.4}$$

where $\gamma_0 \equiv \bar{V}_P \big/ \bar{V}_S = t_{S0} \big/ t_{P0}$, $\gamma_2 \text{£½} V_{P2} \big/ V_{S2}$, where V_{P2} is the short-spread (rms) P-wave velocities and V_{S2} is the S-wave equivalent; and σ is the anisotropy parameter defined by (Tsvankin and Thomsen, 1994) as:

$$\sigma = \left(\frac{V_{p0}^2}{V_{s0}^2}\right)(\varepsilon - \delta) \tag{4.5}$$

In a multi-layered anisotropic model, the conversion-point location is not only affected by the anisotropy, but also by the layering effect. The converted-wave moveout velocity, at every vertical time t_{C0}, is (Thomsen, 1999):

$$V_{C2}^2(t_{C0}) = \frac{V_{P2}^2}{1+\gamma_0} + \frac{V_{S2}^2}{1+\gamma_0} = \frac{V_{P2}^2}{1+\gamma_0}\left(1 + \frac{1}{\gamma_{eff}}\right) \tag{4.6}$$

$$\gamma_{eff} = \frac{1}{(1+\gamma_0) V_{C2}^2 / V_{P2}^2 - 1} \tag{4.7}$$

Here γ_0 is the vertical velocity ratio, and V_{P2} is the short-spread P-wave moveout velocity and V_{S2} is the S-wave equivalent.

Yang and Lawton (2001) mapped the conversion point in VTI media with different anisotropic parameters for a single layer case. The conversion-point location is dependent on the relationship of ε and δ. Here, the conversion-point displacement in VTI relative to its location in isotropic media is also calculated by γ_{eff} method.

From equation (4.4), we can see that if $\delta = \sigma$, then $\gamma_{eff} = \frac{\gamma_2^2}{\gamma_0} = \gamma_0 \frac{(1+2\delta)}{(1+2\sigma)} = \gamma_0$. In this case, $\sigma = \left(\frac{V_{P0}^2}{V_{S0}^2} \right) (\varepsilon - \delta) = \delta$. Thus, we have

$$\delta = \frac{V_{P0}^2 / V_S^2}{1 + V_{P0}^2 / V_S^2} \varepsilon = \frac{\gamma_0^2}{1+\gamma_0^2} \varepsilon . \tag{4.7}$$

When $\gamma_0 = 2$ and $\delta = 0.8\varepsilon$, then $\gamma_{eff} = \gamma_0$. Thus, in this situation and for a single-layer case, the P-S conversion point is located at the same position as that in isotropic case.

This conversion point mapping method is applied on a single-layer VTI model and a three-layer VTI model.

4.2.3 A single-layer VTI model example

First, a single-layer VTI model was created with properties shown in Table 4.1. In this raytracing experiment, the offset ranges from zero to 2000m, which is twice the thickness of the layer.

Table 4.1 One-layer polar anisotropic model with properties defined as shown.

$V_P(0)$	$V_S(0)$	ε	δ	Thickness
3000m/s	1500m/s	0.20	0.10	1000m

This model was raytraced and the $x^2 - t^2$ relationship obtained from raytracing is shown in Figure 4.1. A straight line which represents the hyperbolic case, is plotted for comparison. We can see that the $x^2 - t^2$ curve is non-hyperbolic.

Equation (4.4) was applied to calculate γ_{eff}, the effective velocity ratio of this VTI layer. Then γ in equation (4.3) was replaced by γ_{eff} to calculate the conversion-point location. Figure 4.2 shows the relative location of the conversion point obtained from these two methods. For this example, $\gamma_0 = 2.0$ and $\gamma_{eff} = 1.333$, and $\gamma_0 < \gamma_{eff}$, so the conversion point moves towards the receiver relative to the isotropic case.

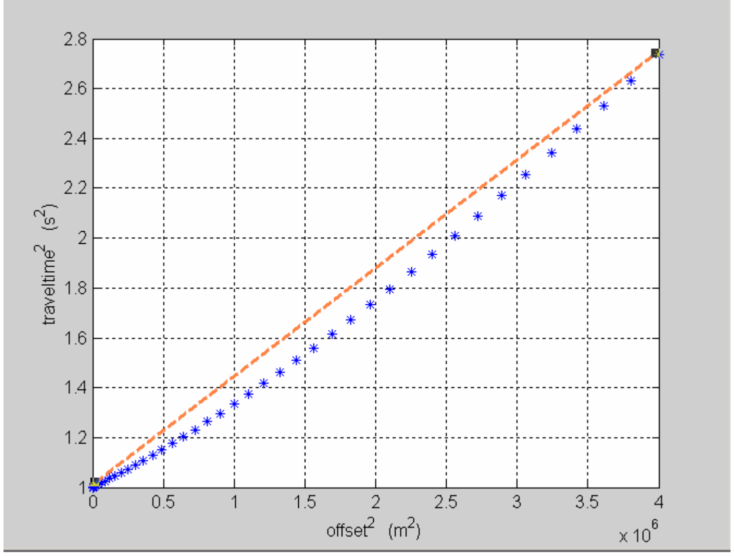

Figure 4.1 The $t^2 - x^2$ curve shows non-hyperbolic moveout.

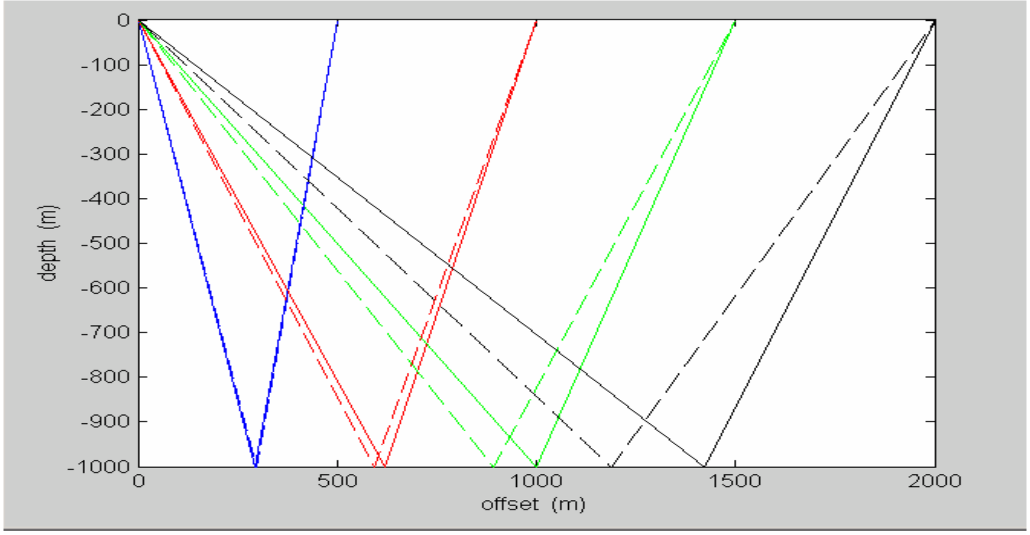

Figure 4.2 Raypaths and the corresponding conversion point location generated from two methods. The solid lines represent the conversion point location obtained from Thomsen's exact equations, where as the dashed line represents the position obtained from γ_{eff} method.

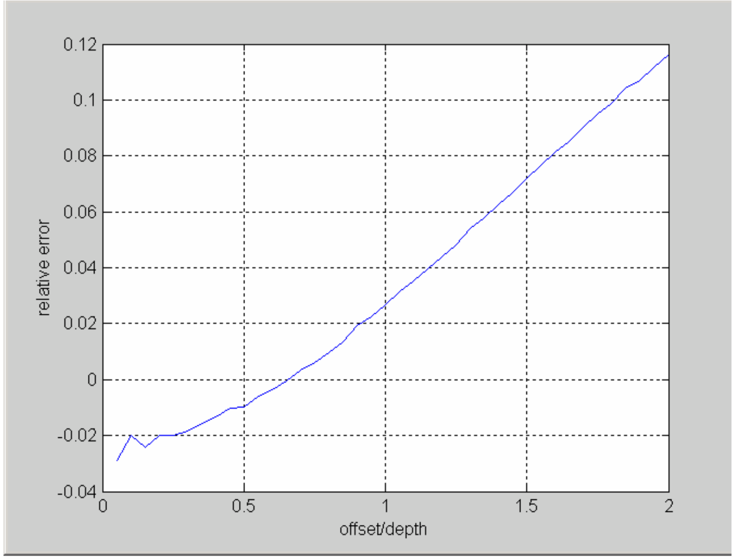

Figure 4.3 Relative error of the conversion point obtained from the γ_{eff} method varying with the offset/depth.

In order to analyze the efficiency of γ_{eff} method, relative error is defined as:

$$error = \frac{x_C^{exact} - x_C^{eff}}{offset}, \tag{4.8}$$

and is plotted verses offset in Figure 4.3. From the display of the relative error, we can see that the γ_{eff} method is sufficient for short-to-intermediate offsets. In a single-layer case for long offset, such as offset-to-depth ratio equals to 2, the relative error reaches 11%.

In the VTI model, the relationship between ε and δ determines whether the conversion point is displaced towards the source or towards the receiver. For the single-layer VTI model, we applied both methods to calculate the displacement of the conversion point from the isotropic case for two different types of anisotropy. Figure 4.4 shows a comparison between the displacements of the conversion-point obtained from these two methods. When $\varepsilon > \delta$, the displacement of the conversion point is negative, which means that the conversion point is displaced toward the source relative to the isotropic case (Figure 4.4 (a)). When $\varepsilon <= \delta$, the displacement of the conversion point is a positive meaning the conversion point is displaced towards the receiver compared to the isotropic case (Figure 4.4 (b)).

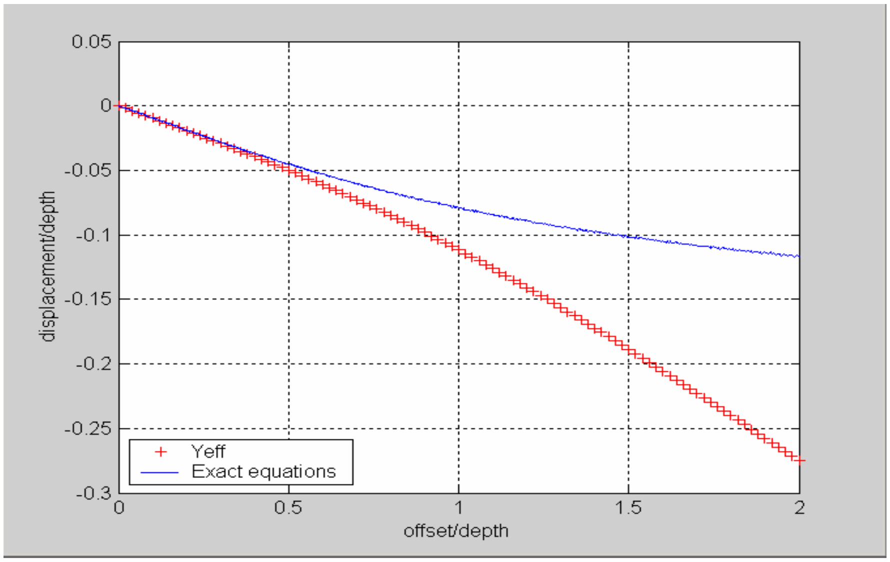

(a)

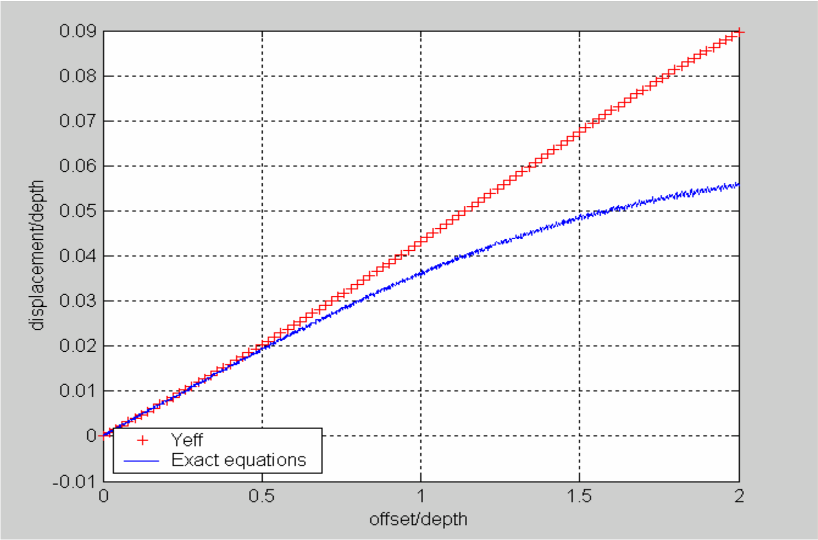

(b)

Figure 4.4 Variation of the conversion-point displacement relative to the isotropic conversion-point as a function of offset/depth, obtained from two methods, at the case of: (a) epsilon=0.20, delta=0.10; (b) epsilon=0.10, delta=0.10, elliptical anisotropy.

4.2.4 Multi-layered model example

A more realistic case, multi-layered VTI model was then studied. A Matlab program was developed for raytracing where the user can define the properties of each layer for modelling. A three-layer model was designed with properties defined for each layer as Table 4.2. The model is of 2000m in thickness, and the offsets ranges from zero to 4000, where the offset/depth reaches two.

Table 4.2 A three-layer polar anisotropic model with properties defined.

Layer	$V_P(0)$	$V_S(0)$	ε	δ	Thickness
1	1500m/s	800m/s	0.20	0.10	1000m
2	2500m/s	1200m/s	0.20	0.15	1500m
3	3300m/s	1900m/s	0.20	0.10	1500m

Similar to the single-layer model experiment, the P-S converted wave was first mapped using Thomsen's exact equations. The $x^2 - t^2$ curve and its best-fit straight line are shown in Figure 4.5; we can see that $x - t$ curve for the P-SV converted wave is non-hyperbolic.

Calculating the slope of the best-fit straight line, we could obtain the converted NMO velocity V_C to flatten the $x - t$ curve with a value of 2090 m/s. Then we shoot P-P rays on this model using the same survey. A similar method was used to compute a P-wave NMO velocity. The average vertical velocity ratio was calculated, and shows $\gamma_0 = 1.91$. Equation (4.7) was used to compute the effective velocity ratio and we get $\gamma_{eff} = 1.384$.

Since $\varepsilon > \delta$ in this model, $\gamma_{eff} < \gamma_0$ and the conversion point moves towards the source compared to the isotropic case. By replacing γ by γ_{eff} in equation (4.3), we calculated the conversion point at the bottom of this model and compare it with the exact location, with results shown in Figure 4.6.

The deviation was calculated using equation (4.8) and the relative error was plotted verses the offset-to-depth ratio in Figure 4.7. We can see that when offset-to-depth ratio equals to 2, the deviation reaches 14% of the offset.

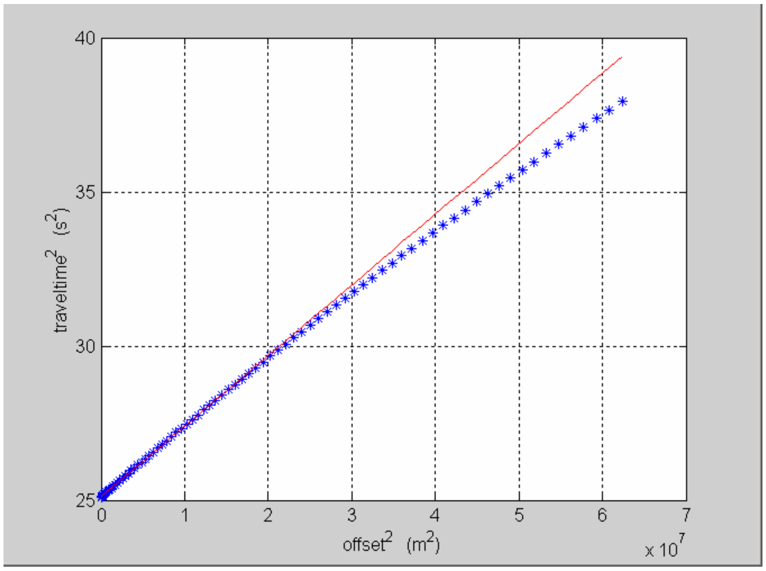

Figure 4.5. The $t^2 - x^2$ curve shows non-hyperbolic moveout in multi-layered VTI media. The straight line is used to obtain the short-spread converted NMO velocity, $V_C = 2134\, m/s$.

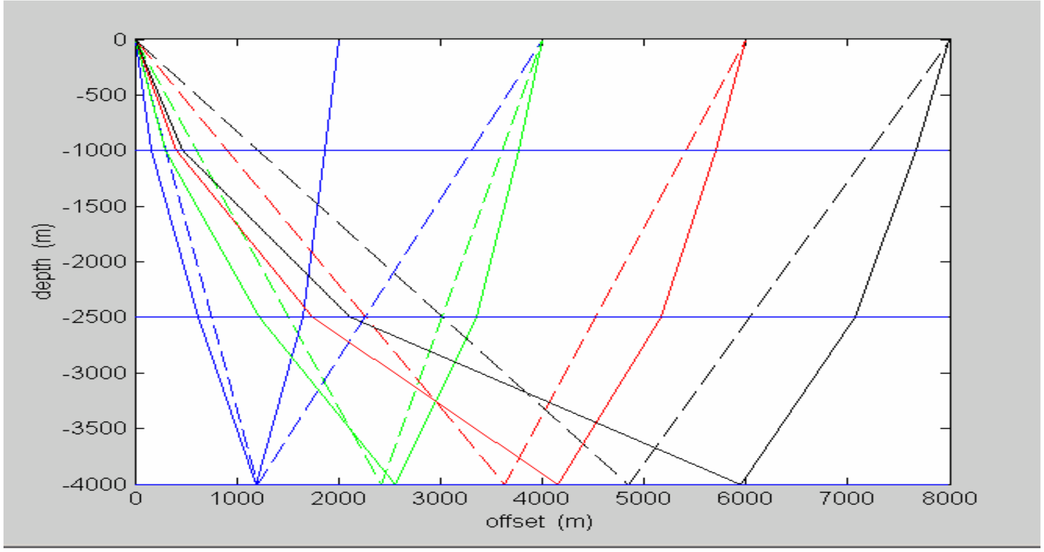

Figure 4.6. The P-S conversion-point position obtained from two methods being applied on the three-layer VTI model. The solid lines show the ray path for certain offsets generated from Thomsen's exact equations and the dashed lines show the conversion-point position by effective velocity with γ_{eff} = 1.384 in isotropic media.

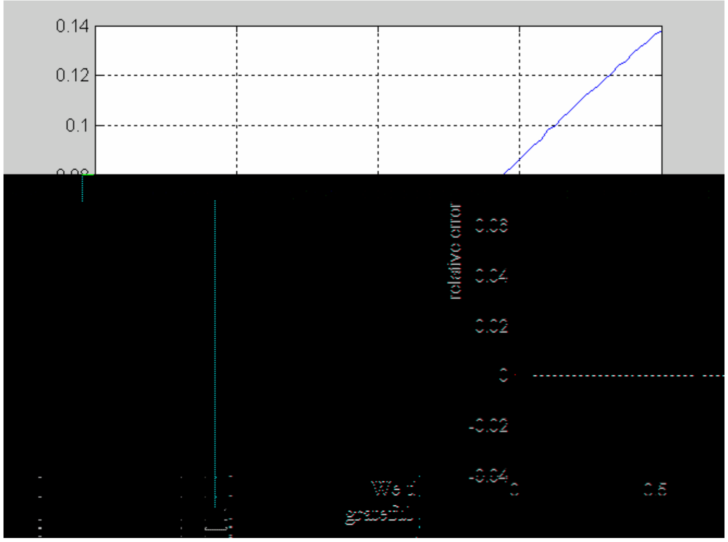

Figure 4.7 The relative error of the conversion point at the base of 3-layer model obtained from the effective velocity ratio method.

4.3 NORSAR 2D anisotropy ray mapping

NORSAR2D is a commonly used forward raytracing tool in seismic exploration research. It also has the capability for raytracing in VTI media, called Anisotropy Ray Mapping (ARM). In this section, a VTI model is created and anisotropic ray-mapping is conducted by using the NORSAR2D ARM to get the displacement of conversion point.

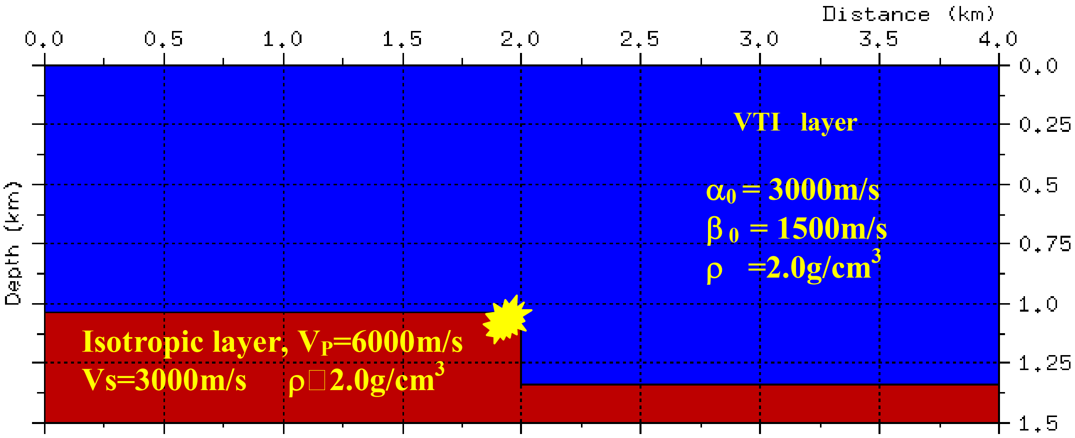

Figure 4.8 The geometry and physical properties of the VTI model designed for NORSAR2D.

The physical parameters $(\alpha_0,\beta_0,\rho,\varepsilon,\delta,\gamma)$ and the size of the model we designed are kept constant as they were defined in Thomsen's equations method. A special point (x = 2.0 km, z = 1.036 km), which is marked with a star, is used to detect the trace number conveniently.

A common-shot survey, with a vertical compression P-wave source and radial S-wave receiver, was conducted in the raytracing on this model.

Synthetic seismograms were generated by NORSAR2D and displayed by ProMAX. In every case the event on the seismogram terminates when the conversion point is located at the step of 2 km. By displaying this seismogram on PROMAX, we know the trace number, so we can determine the offset. An example of the synthetic seismogram is shown in Figure 4.9.

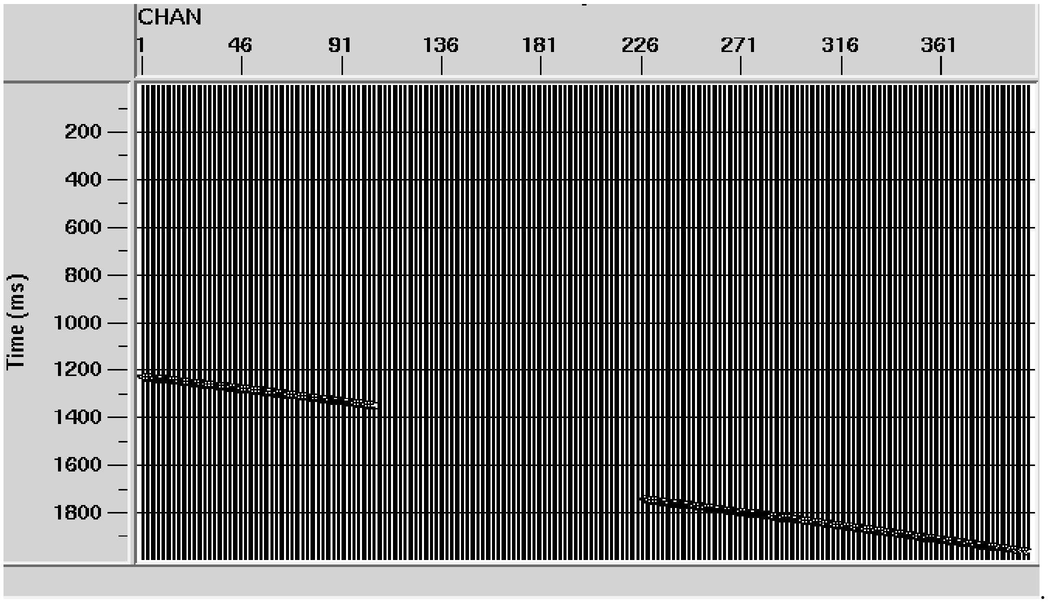

Figure 4.9 An example of P-S wave synthetic seismogram generated from NORSAR2D and displayed in ProMAX.

The horizontal coordinate of the conversion point, X_{p1}, for a certain offset-to-depth ratio is obtained from the display of the synthetic seismogram. The offset of conversion point in the isotropic case, X_{po}, is also obtained by performing common-shot raytracing. The displacement of the conversion point can be obtained by calculating X_{p1} - X_{po}.

The results obtained by using NORSAR2D are shown in Table 4.3 and Table 4.4, for $\varepsilon = 0.10$ and $\varepsilon = 0.20$, respectively. For comparison with the results from our algorithm, the corresponding displacement obtained from the Thomsen's exact equations and linear approximations are also listed together. In this table, '+' sign means the conversion point moves towards the receiver, and '-' means towards the shot.

Table 4.3 Comparison of the conversion point displacement in the VTI model relative to its location in the isotropic case, obtained from NORSAR2D raytracing with that calculated using Thomsen's linear approximations and exact equations. The offset-to-depth ratio is 1.34 and ε = 0.10.

For $\varepsilon = 0.10$	Displacement from NORSAR2D (m)	Displacement from linear equations (m)	Displacement from exact equations (m)
$\delta = 0.20$	236.1	244.18	316.42
$\delta = 0.15$	142.3	139.16	163.58
$\delta = 0.10$	47	41.56	49.53
$\delta = 0.05$	-50	-56.50	-49.39
$\delta = 0.00$	-146	-151.26	-140.15
$\delta = -0.05$	-244	-237	-218.68

Table 4.4 Comparison of the conversion-point displacement in the VTI model relative to its location in the isotropic case, obtained from NORSAR2D raytracing with that calculated using Thomsen's linear approximations and exact equations. The offset-to-depth ratio is 1.34.and ε = 0.20.

For $\varepsilon = 0.20$	Displacement from NORSAR2D (m)	Displacement from linear equations (m)	Displacement form exact equations (m)
$\delta = 0.30$	255	267.69	383.69
$\delta = 0.20$	82	73.70	83.43
$\delta = 0.15$	-4	-18.49	-13.73
$\delta = 0.10$	-171	-103.70	-100.17
$\delta = 0.05$	-180	-189.26	-177.24

From Table 4.3 and Table 4.4, we can see that the results from the NORSAR2D software are close to the ray tracing results obtained from Thomsen's linear equations for weak anisotropy. It has been shown that the value of δ can also have a significant influence on the location of the conversion point.

From Table 4.3 and Table 4.4, we can also see that the results from different methods show the same variation trend. The conversion point in VTI media moves towards the receiver when $\varepsilon \leq \delta$ and towards the shot while $\varepsilon > \delta$. The displacements from the NORSAR2D experiments are much closer to the results from Thomsen's linear equations than to the results from the exact equations.

Chapter five

Physical modeling in a VTI model

5.1 Introduction

In Chapter two, it was shown that the P-S reflection coefficient is dependent on anisotropies above and below the reflecting interface. In chapter three and four, the influence of anisotropies on P-S conversion point location was discussed. In this chapter, the physical modeling experiment on a VTI model will be conducted and analyzed.

Various laboratory and field measurements have shown that anisotropic formation will have a measurable influence on seismic imaging. Isaac and Lawton (1997 and 1998) studied the mislocation in a physical model with a dipping angle of 45°. They showed that the presence of dipping anisotropic beds above the target reflector causes mis-positioning problems when P-wave isotropy is assumed. They found that the target was shifted laterally from its true location. Grech et al. (1999) continued this research on imaging the target beneath the dipping layers using P-wave and S-wave. In their work, four sets of data involving P-wave and S-wave data were acquired from a physical model. The P-wave section exhibits a severe lateral positioning error of 300 m and the converted wave section, have a lateral error of 150m. They concluded that the multi-component data sets might assist with lateral positioning issues in complex thrust belts, where potential hydrocarbon targets often lie.

In order to investigate the influence of VTI layer on the imaging of targets underneath, physical modeling experiments were carried out on a VTI model. The data acquired were then processed and the images were further analyzed.

5.2 Physical modeling

5.2.1 Introduction to physical modeling

Physical modeling is an effective method to simulate a real seismic survey in the laboratory besides numerical modeling (Chen 1994). Due to the inconvenience and cost of the field survey, it is feasible to design and conduct the small-scale seismic survey in the lab. Another advantage of physical modeling is the flexibility of parameter adjustment. It has been proved to be a good way assisting seismic studies by many geophysicists.

In physical modeling experiments, the models are built using materials with different velocities (Phenolic, Plexiglas and aluminium etc.). There are two transducers moving on the surface of the model under the control of a computer. One transducer operates as the source and the other operates as a receiver. The source transmitter stimulates a wavelet signal into the model. The reflected signal data is received and stored in the computer in the same way as conventional seismic recording. The data acquired by physical modeling can then be processed and analyzed to compare with the real field data.

The limitation of physical modeling lies in that the materials cannot be exactly the same as the real sediments. In this chapter, a VTI physical model was constructed and a 2C (P and SV) seismic survey on this model was conducted. The P-P and P-S data were then processed and analyzed to understand P-S conversion point mapping.

5.2.2 Acquisition system overview

The acquisition system used to conduct this experiment was originally developed by CREWES, at the University of Calgary. During the past 10 years, the hardware and software have been incrementally upgraded and now it can be easily manipulated.

The physical modeling system used here consists of several parts shown in Figure 5.1. It mainly includes the transducers as the transmitting and receiving instruments, and the computer as controlling systems (Bland and Macdonald, 1999). A typical trace will be generated by the following steps. The piezoelectric source transducer was excited by a digital wavelet and emits an ultrasonic signal. Then this signal propagates through the model and reaches the receiving transducer. The piezoelectric receiving transducer then converts the mechanical pressure to a very small electrical signal. This signal is then digitized, processed, and stored in the disk. It is well known that the random noise during the acquisition may seriously affect the quality of the data. In order to suppress the noise, the results of 128 stacks of data are summed to generate one trace. We assume that the random noise may cancel or partially cancel due to summation.

After one trace was obtained, the transducers will move into new locations by the controlling computer to shoot a new trace. The receiving transducers can be placed in three directions to record different types of waves (P, SV and SH wave).

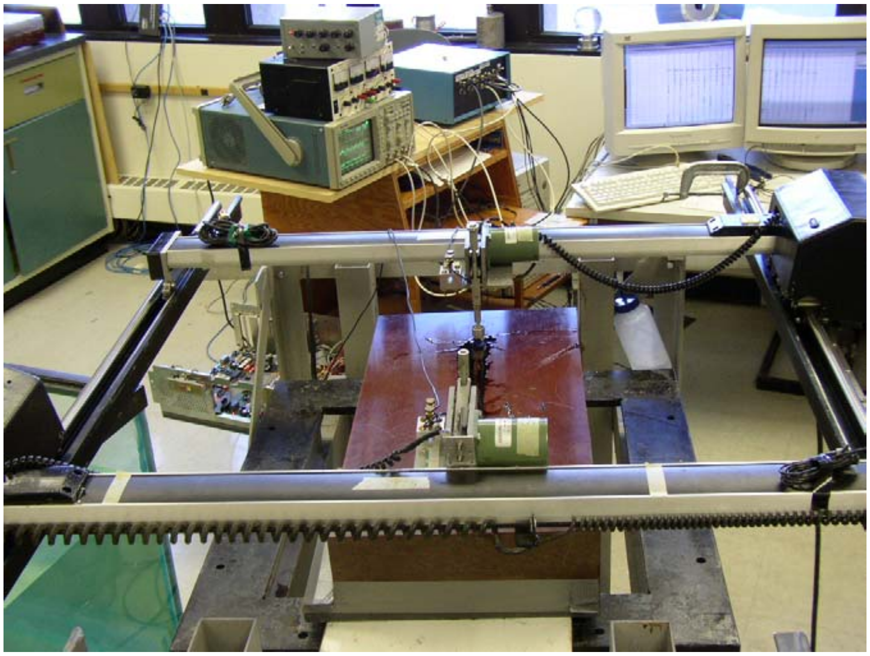

Figure 5.1 The acquisition system used for the physical modeling at the University of Calgary, which mainly includes the transmitting and receiving instruments, and the controlling system.

5.2.3 Model description

In the laboratory, models are constructed by using replacing materials in a certain scale. The scale in our experiment is 1:10,000, which means that 1 mm on the model equals to 10 meters in a real survey. Figure 5.2 shows the photo of the model in this experiment.

The material employed in our experiment to simulate real VTI model is called Phenolic LEB. It is a material made by compressing many layers of linen whose fabric pattern is randomly arranged. Scaled by 10,000, the anisotropic block is 1032 m thick. The slab under the VTI material is made of Phenolic PVC, which is homogeneous and isotropic. The vertical edge of the base slab is used to simulate a reef edge or fault block. The source and receiver transducer are positioned to make the vertical edge located at the centre of the survey line.

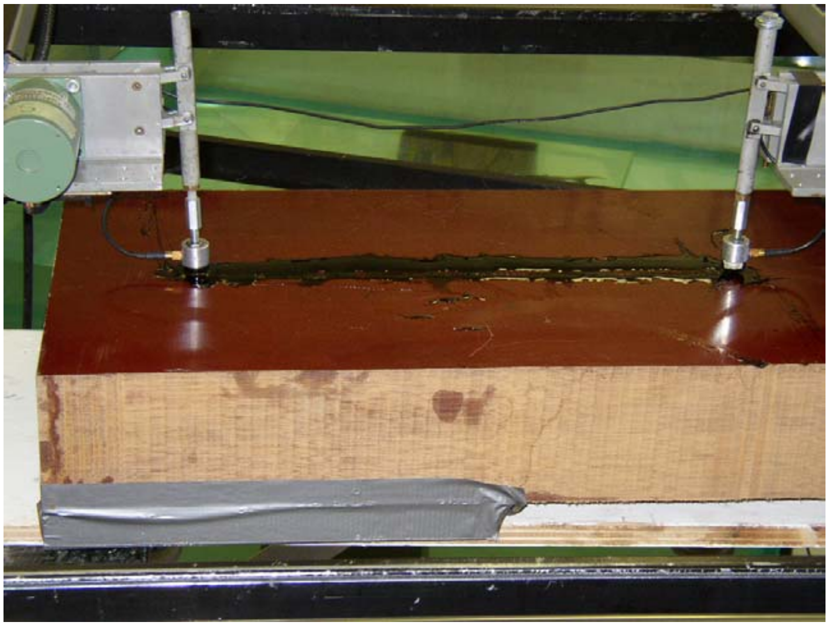

Figure 5.2 The VTI model with an isotropic slab underneath. The two transducers on the surface will be positioned at proper locations according to the commands of the computer.

5.2.4 Calibration

Before the survey is carried out, calibration experiments have to be conducted to determine the properties of the model. A subset of P- and S- wave velocities was measured by transmission of P- and S-waves through the materials at vertical (angle of 0°) and horizontal direction (angle of 90°). P wave was also measured at 45° to calculate the anisotropy parameter δ .

Table 5.1 The P- and S- wave velocities in the model material

	Phenolic LEB	Phenolic PVC
Vp (0°)	2822 m/s	2350 m/s
Vp (90°)	3432 m/s	
V_P (45°)	3053 m/s	
V_{SV} (0°)	1536 m/s	1030m/s
V_{SV} (90°)	1710 m/s	
V_{SH} (0°)	1440 m/s	
V_{SH} (90°)	1504m/s	

The anisotropies of the VTI modeling experiment can be calculated according to Thomsen's definitions, which have been expressed in equation 2.14(a), 2.14(b) and 2.14(c). The anisotropies values of Phenolic LEB are: ε = 0.22 and δ = 0.107.

5.3 Survey design and operation

Different to the normal three-component survey, only a 2C seismic survey (P-P and P-S) survey was conducted in this research. The geometry of the survey is listed below in Table 5.1 (in real world units).

Table 5.2 Geometry of the 2C survey

Source Interval	50m
Receiver interval	10m
Minimum offset	210 m
Maximum offset	4000m

Due to the limitation of the model size, it's not feasible to lay a cluster of receivers on the model and measure the reflection simultaneously. Instead, only one receiver transducer was employed every time to generate one trace. It has to move a distance of one receiver interval along the seismic line consequently to get the rest trace.

5.4 Data processing and analysis

In this section, we will demonstrate the processing flow of P-P data and P-SV data that obtained. Similar processing flows are applied to two datasets, with some additional processing on the P-SV converted wave data.

5.4.1 P-P data

The data acquired from the experiments were exported and transformed into ProMAX format for further processing by the following steps:

SEG-Y data input

Trace header math

Disk Data Output

2D inline Geometry load (CDP binning)

Trace editing

Radial filter and band-pass filter

Velocity analysis

NMO correction

CDP/Ensemble stack

Kirchhoff time migration

Figure 5.3 shows typical P-P and synthetic shot gathers. Due to the fact that the amplitudes of these surface waves are relatively stronger than the P-P reflection signals, it’s hard to identify the events on shot gathers. The synthetic ray tracing experiment is conducted to identify events according to their traveltimes.

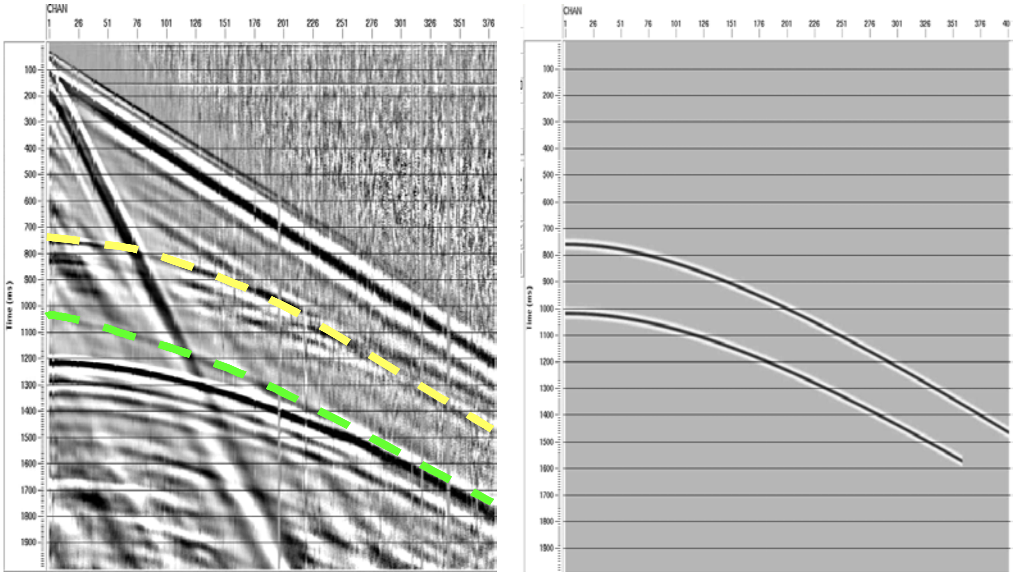

Figure 5.3 A P-P shot gather example (left) with the corresponding synthetic gather generated from Norsar2D (right).

The geometry which matches the data was loaded, and CDP binning was carried out then. Then data were edited with bad traces that are abnormal on the shot gathers being killed to improve the quality of data.

From in Figure 5.3, we can see that the surface waves with constant velocity are dominant in the shot gather shown. Several radial filters are applied here to attenuate the coherent waves whose moveout is linear to the source-receiver offset (Henley, 1999). Figure 5.4 shows shot gather with FFID 39 and 40, before and gathers after the radial filter applied. We find that the radial filters are effective to remove the energy due to the direct wave and surface waves. A band-pass filter with frequency gate values 8-12-40-50 Hz is used to remove the low frequency surface waves.

The P-P velocities were then analyzed and the RMS stacking velocity was picked from the semblances. Then these velocity picked were applied for NMO correction and then CDP stacking. Tsvankin's (1994) long offset correction method was applied during NMO, and anisotropy parameter, η, has to be calculated according to the definition:

$$\eta = \frac{(\varepsilon - \delta)}{(1 + 2\delta)} \tag{5.1}$$

Here in this model, η is 0.12 with ε and δ values calculated in Table 5.1.

Figure 5.5 displays the NMO corrected and stacked P-P section. The diffraction energy from the edge of the isotropic slab is evident on Figure 5.5. Then Kirchhoff time migration was conducted on the stacked section and the migrated image, Figure 5.6, was obtained. By comparison of Figure 5.5 and Figure 5.6, we can see that the diffracting energy are summed and positioned on its true location. The location of the slab edge is located at CDP 401, whose coordinate is at 2000 m. It is exactly located the position in the real model.

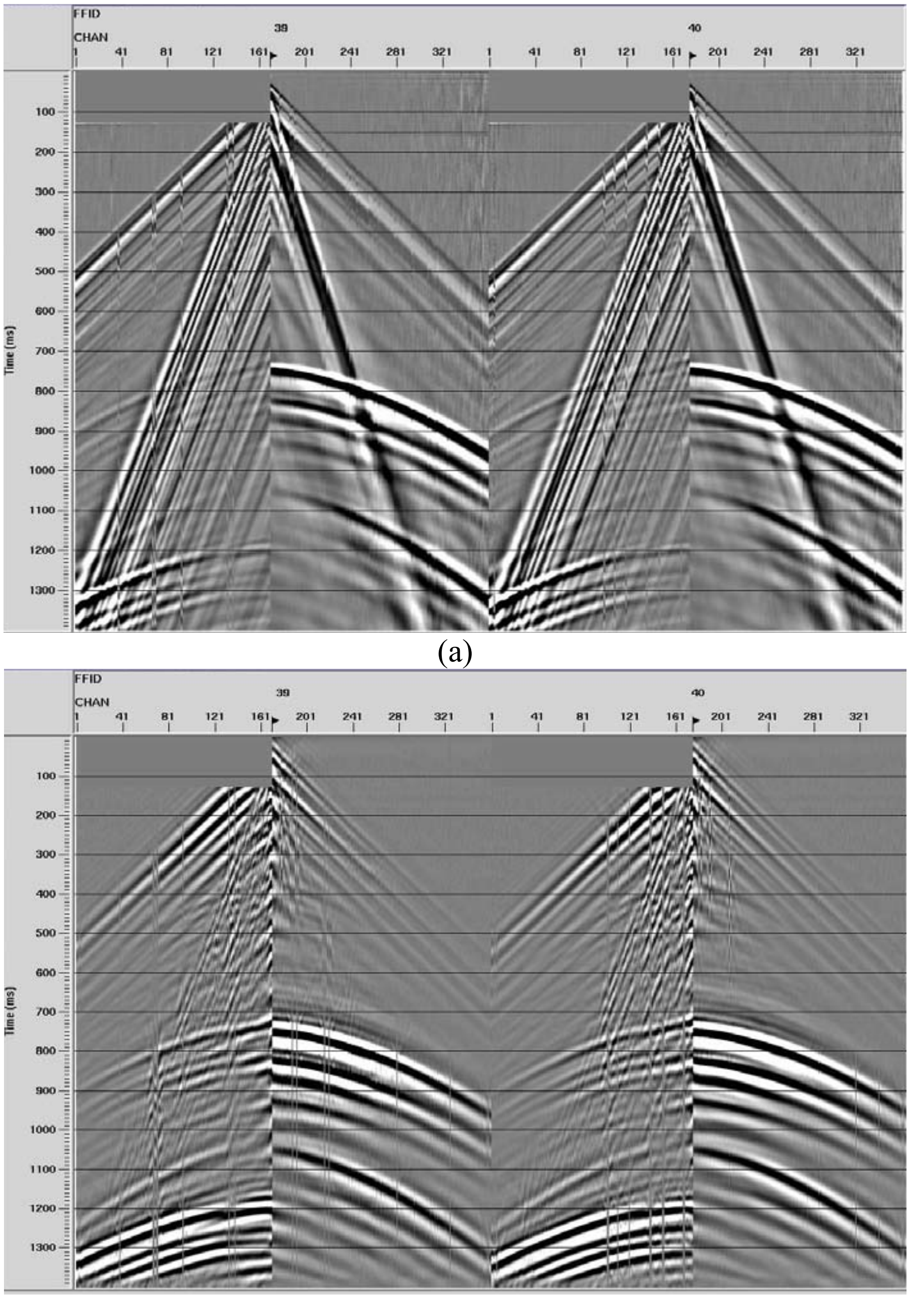

(a)

(b)

Figure 5.4 Two P-P shot gathers before and after radial filter are shown in (a) and (b), respectively. The direct waves and surface waves that are dominant the shot gather in (a) are dramatically decreased after radial filter has been applied.

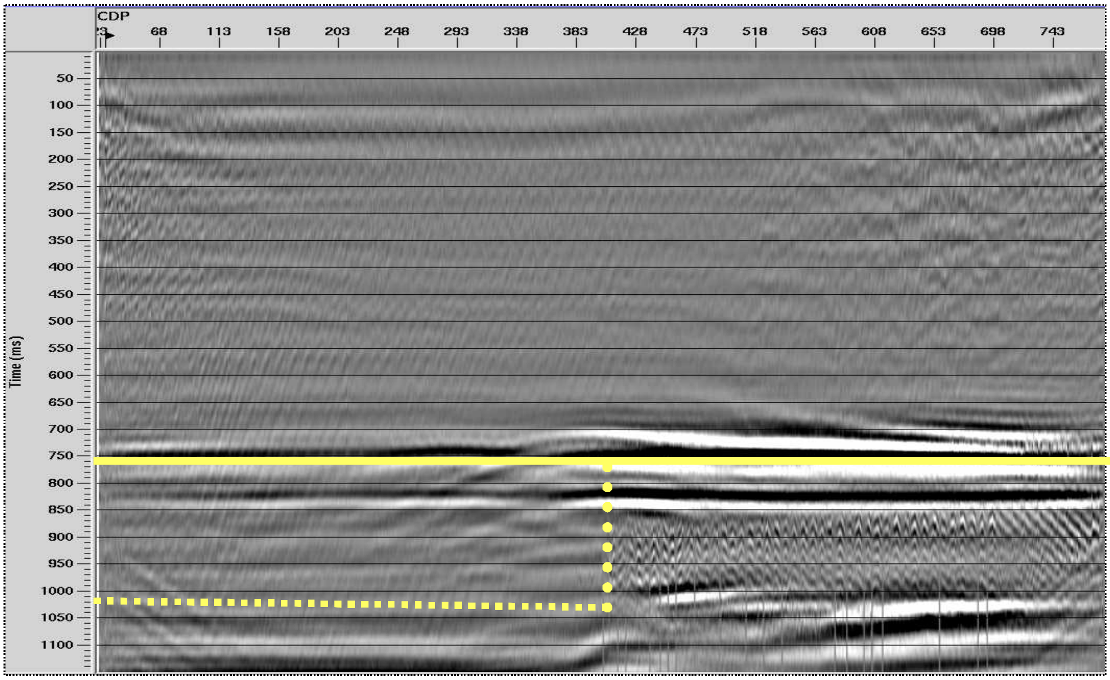

Figure 5.5 NMO corrected and stacked P-P section of the VTI model. The dashed lines show the location of the slab edge on the section located at CDP 401.

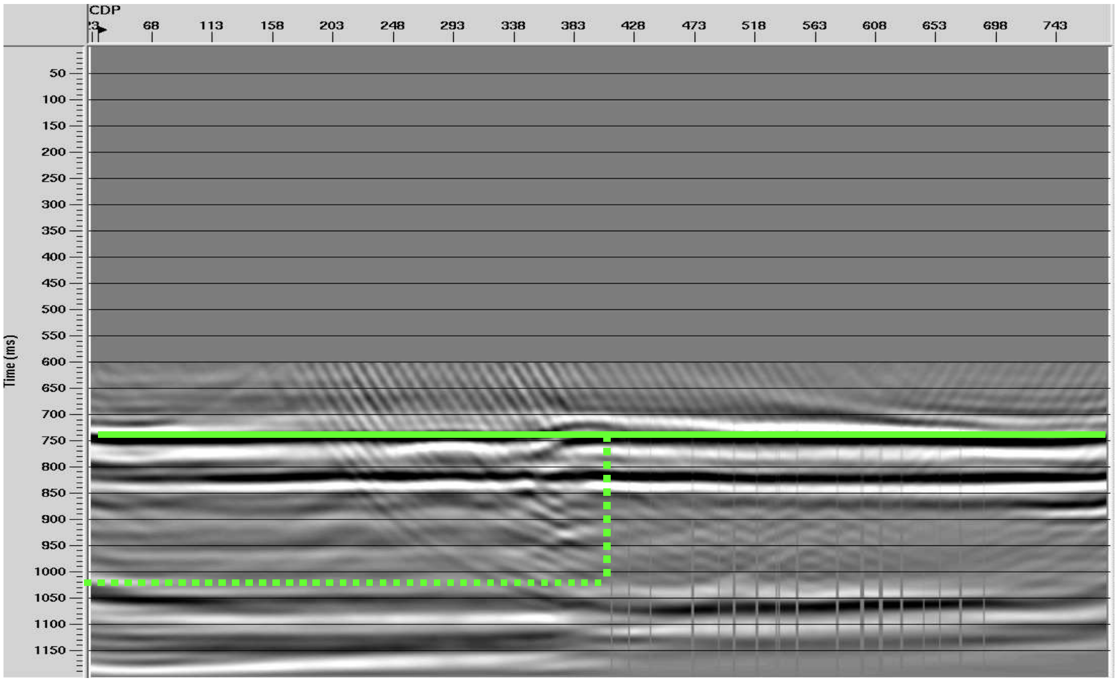

Figure 5.6 Time migrated P-P section of Figure 5.5 where the diffraction energy has been summed together. The dashed line shows the position of the slab edge at CDP 401.

Figure 5.7 shows the NMO corrected and stacked P-P synthetic section. The slab edge location is at CDP 401, too. The location of the isotropic slab edge on the migrated P-P modeling data coincides with that on the stacked synthetic data, and also coincides with the true location. The whole processing is an isotropic processing procedure except the anisotropic long offset correction in NMO correction.

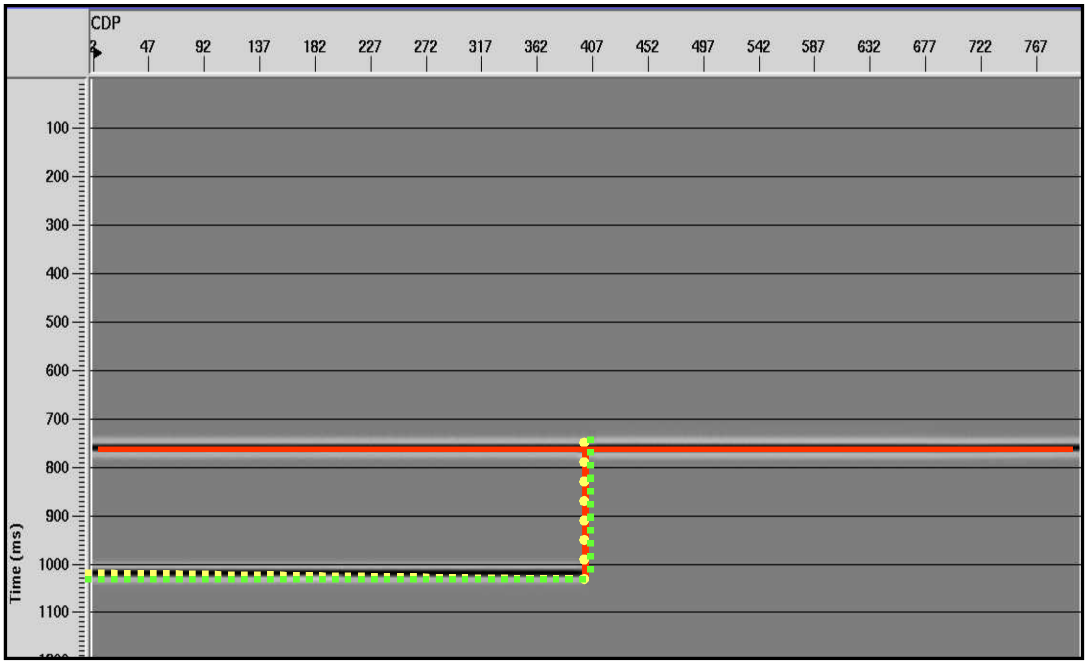

Figure 5.7 NMO- corrected and stacked P-P synthetic section, with the solid red line represents the true location of the slab edge. The dashed lines shown in Figure 5.5 and Figure 5.6 are also shown here for comparison.

5.4.2 P-S data

Similar to P-P data processing stated previously, the P-S converted wave data was processed by using the flow that includes the following steps.

SEG-Y data input
Disk Data Output
2D inline Geometry load (CDP binning)
Trace editing
Asymptotic Conversion point binning
Radial filter, and bandpass filter
Velocity analysis
NMO correction
Converted Wave stack
Kirkchhoff time migration

The main difference between the P-P processing flow and the P-S processing flow lies in the Asymptotic Conversion Point binning and Converted Wave Stack.

A P-S converted wave shot gather example is shown in Figure 5.8, with the synthetic gather shown beside for event identification. From Figure5.8, it is obvious that the gathers are dominated by direct arrivals and surface waves, and the S/N ratio of the P-SV shot gather is very low. We can also see that P- wave events are evident on converted wave gathers, and it is caused by the P-wave energy leakage on the radial transducer. These two main factors cause the poor quality of P-S data. It's hard to identify the P-S events directly. The synthetic P-S converted wave ray tracing experiments are conducted by using Norsar2D to assist the events identification according to their traveltimes.

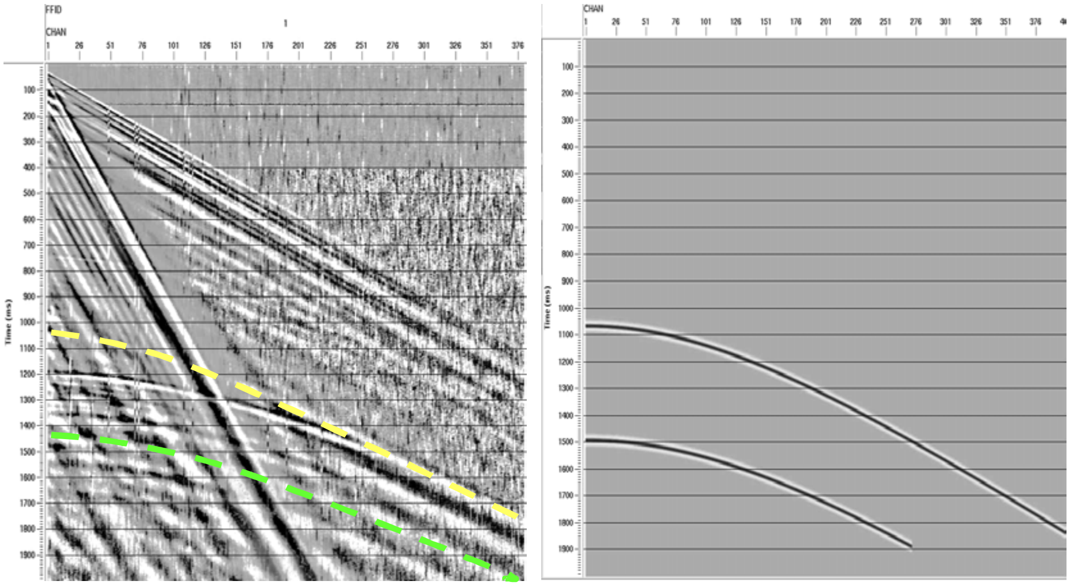

Figure 5.8 A P-S converted wave shot gather example is shown (left) with a synthetic P-S shot gather (right). The P-S events can be identified according to their traveltimes obtained by anisotropic ray tracing in Norsar2D.

Similar to the P-P data processing, several radial filters are also applied into P-SV data processing to remove the coherent waves with constant velocities. Figure 5.9 (a) and (b) show three shot gathers with FFID 39, 40 and 41, before and after radial filtering, respectively. We can see that the radial filters attenuated the coherent waves efficiently and the S/N ratio have been greatly improved. The frequency gate of the bandpass filter used in P-S processing is of 6-10-30-36 Hz.

As discussed in the previous chapters, the P-SV wave data has to be sorted into Common Conversion Point (CCP) gathers. A common conversion point gather is a prestack migration gather that collects all the input traces that contain energy from a conversion point. Asymptotic Conversion Point (ACP) binning is an approximate method, which will cause a great error at high offset/depth ratio, i.e. shallow layers. This error should be corrected by using a different V_P/V_S ratio at shallow layer. Figure 5.10 shows the NMO corrected and stacked section which is conducted after ACP binning.

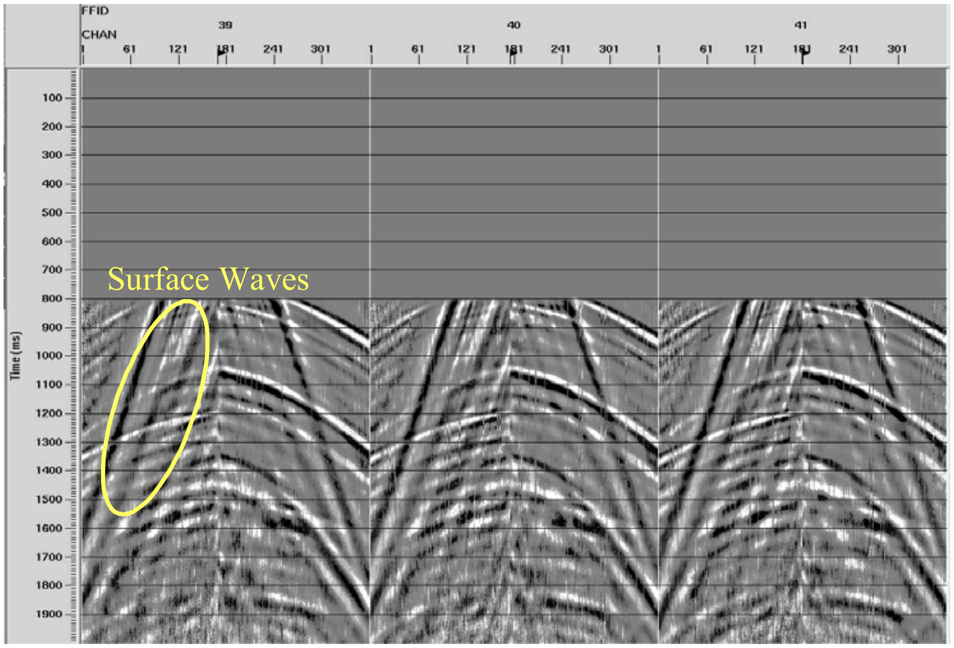

(a)

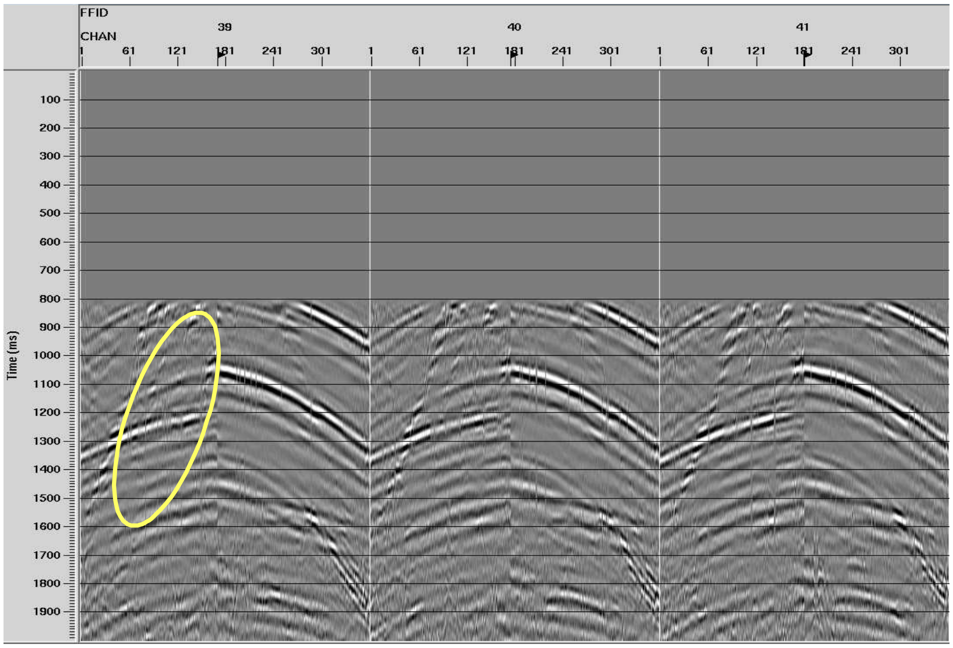

(b)

Figure 5.9 Three shot gathers with FFID 39, 40 and 41 before (a) and after (b) radial filter applied. The surface waves with constant velocities have been attenuated dramatically.

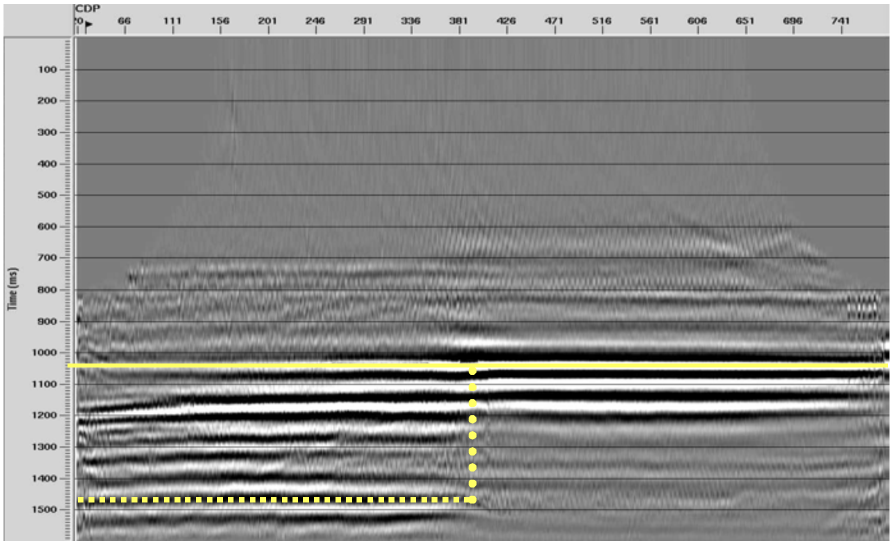

Figure 5.10 NMO corrected and ensemble stacked P-S data section. This section was generated without considering the ACP binning error and anisotropy. The yellow dashed line shows the slab position which is at CCP 409 or coordinate 2040 m.

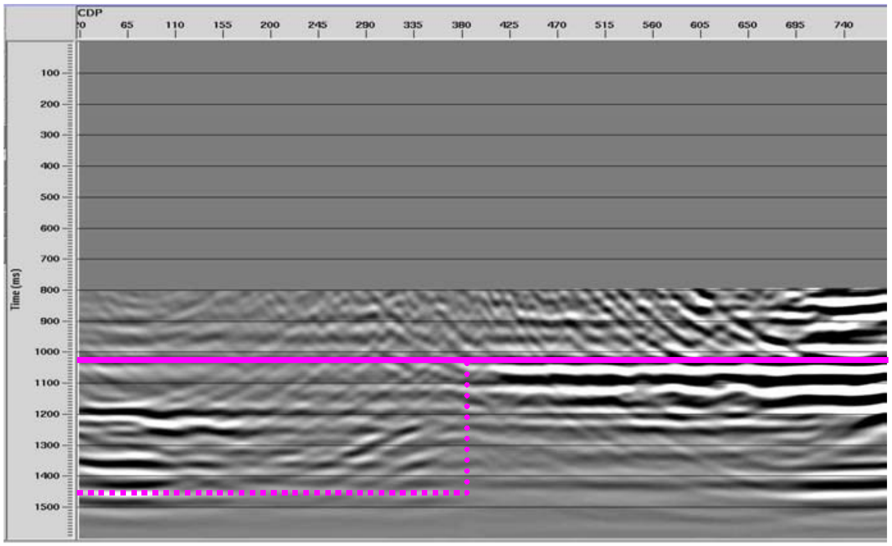

Figure 5.11 The P-S section obtained from converted wave depth-variant stack and then Kirchhoff time migration. The dashed lines address the edge of the isotropic slab underneath the VTI layer, which is at CCP 397, or coordinate 1980 m.

Since the top layer is VTI layer, anisotropy that may cause mis-positioning has to be considered as well. The ACP error and anisotropic error are taken into account by using an equivalent velocity ratio, which is discussed in Chapter four. The depth-variant converted wave stack is applied, with velocity ratio varying with different time. The migrated section of P-S converted wave is then generated and displayed in Figure 5.11.

The P-S Synthetic data obtained from Norsar2D is also processed using the P-S processing flow and the stacked section is shown in Figure 5.12. The solid red line represents the true location of isotropic slab edge at CCP 401, or coordinate 2000 m. The two slab positions shown on the previous two sections are also shown together for comparison.

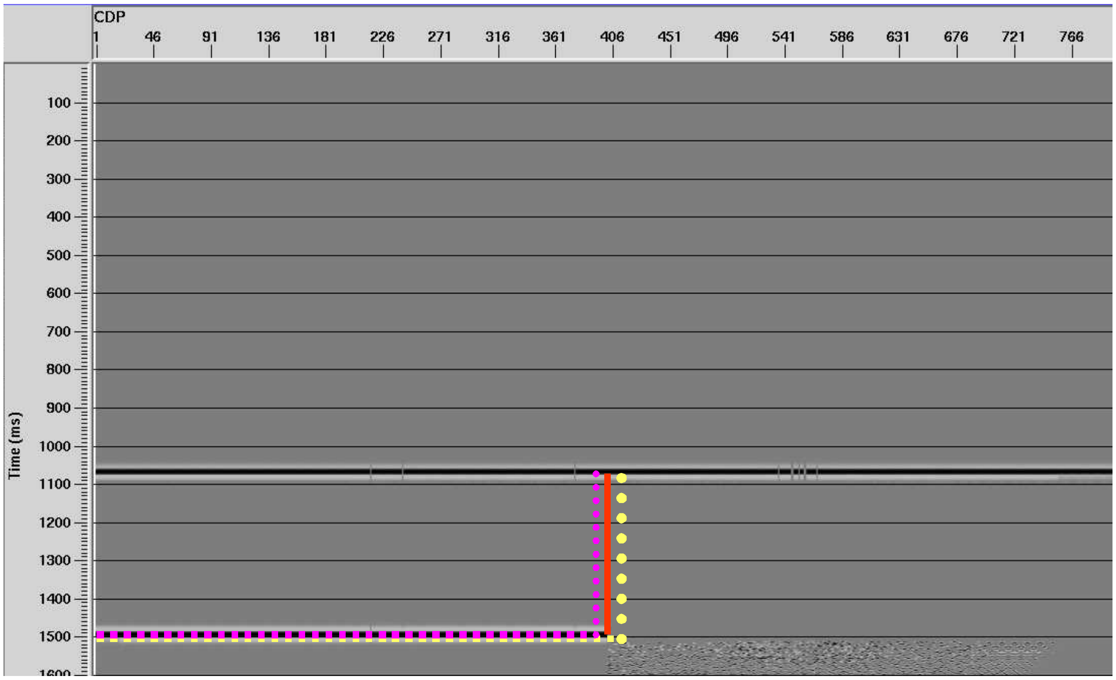

Figure 5.12 The P-S synthetic stacked section with solid lines stands for the true location of the slab edge. The slab locations from isotropic stacking method, and the converted wave stacking method, are also shown for comparison.

5.5 Discussion

The P-P and P-S data acquired from the experiments are processed using ProMAX. The NMO stacked and migrated section shows the location of the isotropic slab edge underneath the VTI layer. This processing flow does not include anisotropic corrections except the NMO correction. The image shows that the slab edge location mapped from this isotropic method coincides with its true location. This means that the overburden VTI layer does not have significant influence on P-P imaging.

The P-S data were processed using two different methods. Firstly isotropic NMO correction and CDP stack was undertaken. In this method, it does not take account of the VTI layer. The other is converted wave stacking and migration, which include the influence of anisotropy by using an equivalent velocity ratio. There exist lateral displacements between these methods and the true location. The slab edge position obtained from the isotropic processing flow is located at +40 meters from the true position. According to Chapter 4, when ε is greater than δ, the conversion point is located towards the source compared to that of isotropic case. So when isotropic processing algorithm is applied, the conversion point is located towards the receiver, relative to its true location. The equivalent velocity ratio method can image the slab edge location better than the isotropic method, with a –20 m error.

Chapter six

Discussion and Conclusions

The earth is known to be anisotropic, although basic seismic survey planning and data processing are based on the isotropic assumption. The VTI case is the most commonly considered type of anisotropy. In this thesis, both numerical and physical modeling of P-SV converted wave experiments were conducted on a VTI model. The general conclusions based on the thesis research are summarized in this chapter.

6.1 Numerical modeling

The reflection coefficients for P-P and P-SV waves were calculated for two VTI models and compared with the isotropic case. We found that the P-P reflectivity in VTI is lower than that for the isotropic case, but the P-SV reflectivity is larger than that in the isotropic case when the wave propagates from a lower impedance layer to a higher impedance layer. The critical angle in the VTI case is greater than that for isotropic case for equivalent vertical velocities. When the incident P-wave travels from high impedance layer to low impedance layer, the P-S reflectivity is smaller than that in isotropic case.

The P-SV conversion point location is of great importance in converted wave survey design and data processing. The important aspect of converted-wave (P-S) seismology is that the exact location of P-S conversion point at the reflector is not well known. Unlike the midpoint determination in P-P wave exploration that is determined geometrically, the conversion point in P-S exploration is determined by physical properties of the formations. In practical processing, it is obtained by calculation, followed by depth-variant sorting. The depth-dependent conversion-point position is often approximated by asymptotic conversion point, which is at a constant offset to the source.

When the formation is shown to be anisotropic, the conversion point cannot be approximated by the position found in the isotropic case. The horizontal displacement of the conversion point in VTI media from that in the isotropic case was mapped by using Thomsen's angle-dependent velocity equations and angle equations, both the linear approximation and the exact forms. The following conclusions are drawn from the conversion point mapping experiments.

1. It is found that the location of P-S conversion point in VTI media depends on anisotropic parameters, P- to S- velocity ratio, and offset/depth. The relationship linking the displacement and the anisotropic parameters, and offset-to-depth ratio and velocity ratio can be complicated.

2. The displacement of the conversion point from that in isotropic case increases with the increasing offset-to-depth ratio and Thomsen's (1986) anisotropic parameter ε. The value of δ can also have a significant influence on the displacement of the conversion point.

3. When ε is larger than δ, for the same offset, the conversion point moves towards the source in VTI media relative to that in the isotropic case. When ε is less than or equal to δ, then for same offset, the conversion point moves towards the receiver.

4. The velocity ratio doesn't have a significant influence on the displacement of the conversion point for small offset/depth, but has influence on for large offset/depth.

5. There is no significant difference between the results obtained from Thomsen's exact equations for anisotropic velocities and ray-angle calculations, and the results from the linear-approximation equations for small offset-to-depth ratios. The difference becomes significant for offset-to-depth ratios greater than 1.5.

Besides the method using Thomsen's velocity equations, the P-S conversion point was also calculated by using the γ_{eff} method. Here, γ_{eff} refers to the effective velocity ratio, which is assumed to account for anisotropy. Both methods were applied for a single-layer model as well as on a three-layer model. The relative error of using γ_{eff} was also calculated for both models to study the efficiency of the γ_{eff} method. In the single-layer model and multi-layered model, the relative error is less than 8% for short-to-intermediate offsets (offset-to-depth ratio less than 1.5). The relative error increases with the increasing offset in both models. For long offsets, i.e. offset-to-depth ratio greater than 2, the γ_{eff} method is an insufficient approximation for mapping the P-S conversion-point.

A commercial raytracing software package, NORSAR2D, was also applied to map the P-SV converted wave. The results were compared with the displacements that were obtained by using Thomsen's equations. The results from NORSAR2D software is close to the results obtained from Thomsen's linear equations for weak anisotropy.

6.2 Physical modeling

Physical seismic modeling experiments on a VTI model were conducted in the CREWES laboratory at the University of Calgary. The model consists of two parts, a VTI layer and an isotropic slab underneath. The edge of the isotropic slab is used to simulate a fault or channel (or reef) edge. P-P and P-SV surveys were undertaken over this model.

The P-P data processing flow does not include anisotropy except for NMO correction. The image shows that the slab edge location mapped from this isotropic method coincides with its true location. This means that the overburden VTI layer does not have significant influence on P-P imaging.

P-SV data were processed using ProMAX by using two methods. The first assumes velocity isotropy. When NMO correction and CCP stacking was applied, the slab edge position obtained is located at +40 meters from the true position. The second approach involved using converted wave stacking and migration, including the influence of anisotropy by using an equivalent velocity ratio. This method imaged the slab edge location with a 20 m error and it is better than the isotropic method.

When the synthetic P-SV data obtained from Norsar2D anisotropic ray mapping was processed, the converted wave stack method imaged the slab edge at its true location. The location of the slab edge on the imaged synthetic section assuming isotropy shows an error of –5 m.

REFERENCES

Alkhalifah, T., Larner, K., 1994, Migration error in Transversely Isotropic media, Geophysics, Vol. 59,No.9, P: 1405-1418

Anderson, B., Helbig, K., Bryant, I., Luling, M., and Spies, B., 1994, Oilfield anisotropy: Its origins and electrical characteristics, Oilfield Review, October, 48-56.

Backus, G. E., 1962,Long-wave elastic anisotropic produced by horizontal layering: J. Geophys. Res., 67, 4427-4440.

Berryman, J. G., 1979, Long-wave elastic anisotropy in transversely isotropic media: Geophyics, 44, 896-917

Bland, H., and Macdonald, P., 1999, Software for physical modeling design and acquisition, CREWES Research Report, Vol11.

Brown, R. J., 2001, course notes for the course *Converted wave Exploration* at the University of Calgary.

Chen, T., 1994, Multiconverted reflections in marine environments with thin permafrost layers, M.Sc thesis, University of Calgary.

Cordsen, A. and Lawton, D. C., 1996, Designing 3-component 3-D seismic surveys, 66th Ann. Internat. Mtg: Soc. of Expl. Geophys., 81-83.

Crampin, S., 1977, A review of the effects of anisotropic layering on the propagation of seismic waves: Geoph. J. R., astr. Soc., 49, 9-27

Crampin, S., 1985, Evaluation of anisotropy by shear-wave splitting: Geoph., 50, 343-391

Daley, P.F., and Hron, F., 1977, Reflection and transmission coefficients for transversely Isotropic media: Bull., Seis. Soc. Am., 67, 661-675

Gaiser, J. E., 2000, Advantages of 3-D PS-wave data to unravel S-wave birefringence for fracture detection: 70th Ann. Internat. Mtg., Soc. Expl. Geophys., Expanded abstracts,1201-1204.

Garrota,R., Marechal, P., and Magesan,M.,1985, Two-component acquisition as a routine procedure for recording P-waves and converted waves: Can. J. Expl.Geophys., 21,40-53.

Grech, M. G. K., Isaac, J. H. and Lawton, D. C., 1999, Poster Paper -- Comparison of structural imaging in anisotropic media using P-wave and S-wave data: THE LEADING EDGE, **18,** no. 9, 1062-1066

Helbig, K., 1979, Discussion on "The reflection, refraction and diffraction of waves in media with elliptical velocity dependence" by F.K. Levin: Geophysics, 44, 987-990.

Helbig, K., 1986, Shear-waves-what they are and how they can be used, Soc. Exploration Geophysicist, reprinted, 5-22.

Henley, D. C., 1999, Coherent noise attenuation in the radial trace domain: introduction and demonstration, CREWES research report, Vol. 11, p455-491

Isaac, J. H., Lawton, D. C., 1997, Anisotropic physical modeling, FRP research report, Vol 3, 15-1

Isaac, J. H., Lawton, D. C., 1998, Multicomponent anisotropic physical modeling, FRP research report, Vol14, 9-1

Isaac, J. H., Lawton, D. C., 1999, Image mis-positioning due to dipping TI media: A physical seismic modeling study, Geophysics, Vol 64, No.4, P-1230-1238

Krebes, E. S., Seismic Theory and methods, GOPH551 course notes

Larner, K., and Cohen, J. K., 1993, Migration error in transversely isotropic media with linear velocity variation in depth: geophysics, 58, 1454-1467.

Lawton, D.C., and Cary W. P., 2000, Conversion point mapping and interpolation in P-S survey design, CREWES Annual Research Report, Volume 12, 53-62

Lawton, D.C., Hoffe, B., and Cary W.P., 2000, Some design issues for 3D P-S seismic survey, SEG/EAGE Summer Research Workshop

Li, X., Kuhnel, T., and Macbeth,C., 1996, converted-wave AVO and its implications:58th Ann. Conf., Eur. Assn. Geosci. Eng., Extended abstracts, M046

Li, X., Yuan, J., Ziolkowski, A., and Strijbo, F., 1999, Estimating V_P/V_S ratio from converted waves-a 4C case example: 61st Ann. Conf., Eur. Assn. Geosci. Eng., Extended Abstracts, P066.

Miller, S.L. M., and Stewart, R.R., 1990, The effects of lithology, porosity and shaliness on P-and S-wave velocities from sonic logs: Can J. Expl. Geophys, 26,94-103.

Nye, J.F., 1957, Physical properties of crystals: Oxford Press.

Sheriff, R., 2002, Encyclopedic of dictionary of applied geophysics.

Stewart, R.R., 1999, 3-D multi-component survey design: P-P versus P-S fold: CREWES research report, Vol 11, 207-210.

Stewart, R.R., and Todorov, T., 2000, Oil volume estimation using 3C-3D seismic data well logs: Presented at SEG/EAGE Summer Research Workshop, Boise, Idaho.

Stewart, R.R., Gaiser, J.E., Brown, R.J., and Lawton, D.C., 2002, Tutorial -- Converted-wave seismic exploration: methods, Geophysics, Vol67, No.5, P1348-1363.

Stewart, R.R., Gaiser, J.E., Brown, R.J., and Lawton, D.C., 2003, Tutorial --- Converted-wave seismic exploration: applications, Geophysics Vol. 68, No.1, P: 40-57.

Tatham, R.T., 1882, V_P/V_S and lithology: Geophysics, 47, 336-344.

Tessmer, G., and Behle, A., 1988, Common reflection point data-stacking technique for converted waves, Geophysical Prospecting, Volume 36, 671-688.

Tessmer, G., Krajewski, P., Fertig, J., and Behle, A., 1990, Processing of PS reflection data applying common conversion-point stacking technique, Geophysical Prospecting, Volume 38,267-286.

Tessmer, G., and Behel, A., 1990, Conversion Points and traveltimes of converted waves in parallel dipping layers, Geophysical prospecting, Volume 39, 387-405.

Thomsen, L., 1986, Weak elastic anisotropy: Geophysics, Vol.51, No.10, 1954-1966.

Thomsen, L., 1999, Converted-wave reflection seismology over inhomogeneous, anisotropic media: Geophysics, 64, 678-690.

Thomsen, L., 2002, Understanding Seismic Anisotropy in Exploration and Exploitation: SEG 2002 DISC Series, No.5.

Tsvankin I., and Thomsen L., 1994, Nonhyperbolic reflection moveout in anisotropic media: Geophysics, **59**, 1290-1304.

Vestrum, R., Lawton, D. C., and Schmid., R., 1998, Imaging structures below dipping TI media, Geophysics, Vol64, No.4: P1239-1246.

Winterstein, D. F., 1990, Velocity anisotropy terminology for geophysicists: Geophysics, 58, 1070-1088.

Yang, J., and Lawton, D.C., 2001, Mapping the P-S Conversion point in Vertically Transverse Isotropic (VTI) media, CREWES report, Vol.13, 680-697.

Yang, J., and Lawton, D. C., 2002, Comparison between two P-S conversion point mapping approaches in VTI media, Vol. 14.

.